PERGAMON

Deep-Sea Research II 48 (2001) 419–456

DEEP-SEA RESEARCH
PART II

www.elsevier.com/locate/dsr2

A 3-D prognostic numerical model study of the Georges Bank ecosystem. Part I: physical model☆

Changsheng Chen[a,*], Robert Beardsley[b], Peter J.S. Franks[c]

[a]*Department of Marine Sciences, The University of Georgia, Athens, GA 30602-2206, USA*
[b]*Department of Physical Oceanography, Woods Hole Oceanographic Institution, Woods Hole, MA 02543, USA*
[c]*Marine Life Research Group, Scripps Institution of Oceanography, University of California, San Diego, La Jolla, CA 92093-0218, USA*

Received 8 December 1998; received in revised form 4 September 1999; accepted 15 February 2000

Abstract

The influence of tidal forcing and tidal and wind mixing on circulation and stratification over Georges Bank and adjacent regions in the Gulf of Maine has been examined using the 3-D semi-implicit version of the Blumberg and Mellor (1987) primitive equation ocean-circulation model. The numerical domain covered the Gulf of Maine/Georges Bank region with an open boundary starting at the New Jersey coast and ending at the Nova Scotia coast, with increased spatial resolution over Georges Bank. Numerical experiments were conducted using both smoothed and non-smoothed high-resolution (15 s) bottom topography. The model was forced by specifying the M_2 elevation and phase on the open boundary, and several forms of the bottom roughness parameter z_o were used. The model provided a reasonable simulation of the M_2 tidal elevations and currents. The model, when run as an initial value problem with early summer stratification, exhibited tidal mixing fronts around the 40–60 m isobath over Georges Bank and Nantucket Shoals, and 100-m isobath on Brown Bank. The formation of these tidal mixing fronts significantly enhanced the along-isobath tidal rectified current over Georges Bank and the other two shoal regions. A cool-water band developed within the frontal zone along the eastern and southern flanks of Georges Bank and Nantucket Shoal, and it became cooler owing to wind mixing and upwelling as a mean summer wind stress was added. Tidal mixing and turbulent dissipation varied in time asymmetrically over Georges Bank. Over Georges Bank, tidal mixing was generally characterized as a local 1-D balance between turbulent shear production and dissipation. The spatial structure of the tidal residual flow and local turbulent dissipation rate depended critically on the spatial resolution of the bottom topography and the spatial distribution of z_0. Analysis of the 3-D momentum balance and the residual flow over the center of Georges Bank indicates that earlier results based on a 2-D cross-bank model correctly captured the basic dynamics of stratified tidal rectification and tidal mixing in this idealized model setting. © 2000 Elsevier Science Ltd. All rights reserved.

☆ Paper published in December 2000.

* Corresponding author. Tel.: + 1-706-542-1604.

E-mail addresses: chen@whale.marsci.uga.edu (C. Chen), rbeardsley@whoi.edu (R. Beardsley), pfranks@ucsd.edu (P.J.S. Franks).

0967-0645/01/$ - see front matter © 2000 Elsevier Science Ltd. All rights reserved.
PII: S0967-0645(00)00124-7

1. Introduction

We recently have extended our 2-D coupled physical/biological model (Franks and Chen, 1996) to cover the Georges Bank and Gulf of Maine domain. This 3-D-coupled model includes new high-resolution topographic data and can be run as an initial value problem starting with different stratification, nutrient, phytoplankton and zooplankton distributions to test various ideas about fundamental processes in this ecosystem. As an initial test of this new model, we will focus in this first paper (Part I) on the physical processes that influence the formation of tidal mixing fronts and stratified residual flow over Georges Bank. A second paper (Part II) will present the model-predicted biological fields (Franks and Chen, 2001). A brief introduction to the study region will be given next.

The Gulf of Maine (GOM), located between Cape Cod and Nova Scotia, is a semi-enclosed basin opening to the North Atlantic Ocean (Fig. 1). The GOM topography is characterized by several deep basins and shallow submarine banks (Fig. 2a). The largest bank is Georges Bank (GB), which is separated from Nantucket Shoals (NS) to the west by the Great South Channel (GSC) and from the Scotian Shelf to the east by the Northeast Channel (NEC). GB is roughly elliptical in plane view, with a length of about 200 km along the major axis and a width of about 150 km along the minor axis. The cross-bank bottom topography rises steeply with a slope of about 0.01 from 1000 m on the upper slope to 100 m at the shelf break, then increases slowly with a slope of roughly 0.001–40 m over a distance of about 75 km towards the crest of the bank, and

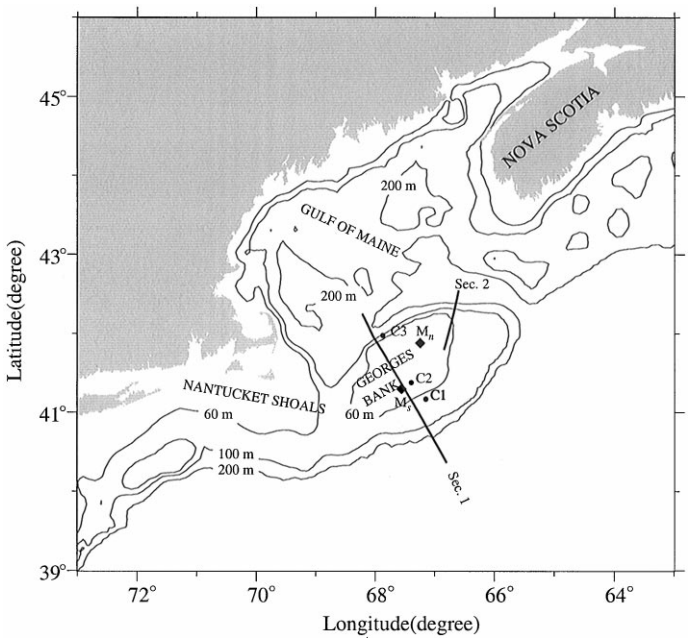

Fig. 1. Bathymetry (in meters) of the southern New England continental margin. The heavy solid lines are the two sections (Sections 1 and 2) used to present the cross-bank distribution of currents and stratification in the paper. Filled diamond symbols locate the turbulent microstructure measurement stations made by Horne et al. (1996) (M_n) and Burgett (1997) (M_s). C1, C2, and C3 are three reference stations used to describe model time series.

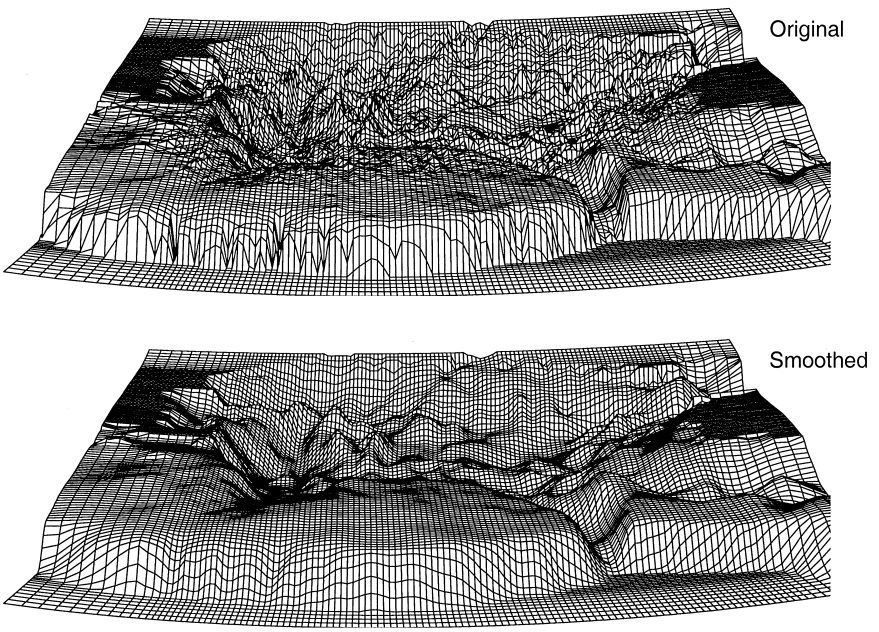

Fig. 2. 3-D views of the original non-smoothed (15 s) and smoothed bottom topographies used in our model experiments.

then decreases rapidly with a slope of about 0.03 to a depth of 300 m in the deep basin just north of the bank crest.

The first systematic study of general circulation in the GOM was conducted by Bigelow (1927), who suggested that the summer surface flow was dominated by two relatively large-scale gyres: a cyclonic circulation around Jordan and Wilkinson Basins to the north of GB and an anticyclonic (clockwise) flow around GB. The Butman et al. (1982) summary of moored Eulerian current measurements confirmed the mean clockwise flow around GB, and showed a southward flow along the southeast coast of Cape Cod. Recent Lagrangian measurements, conducted using satellite-tracked drifters with drogues at 5 and 50 m, clearly illustrated the closed nature of the around-bank clockwise circulation on GB during summer (Limeburner and Beardsley, 1996) (denoted L&B). These drifters showed a large seasonal change in residual circulation over GB. During summer, they tended to move clockwise within or close to the tidal mixing frontal zone around GB, and frequently made several complete circuits over several months. In fall and winter, the drifters tended to leave GB within a few weeks.

Loder (1980) used an analytical model to show that the clockwise residual circulation over GB is due to rectification of the strong semidiurnal tidal currents over the bank's variable topography. This mechanism was further demonstrated by Greenberg (1983) using a vertically averaged barotropic numerical model and by Lynch and Naimie (1993) using a 3-D finite-element model with realistic GOM/GB topography. The summer intensification of the clockwise circulation is believed due, in part, to seasonal development of the tidal mixing front (Loder and Wright, 1985; Chen and Beardsley, 1995), nonlinear interaction of internal waves near the fronts, and modification of internal friction by stratification (Chen et al., 1995a). This seasonal circulation pattern was

simulated diagnostically by Naimie et al. (1994) and later prognostically by Naimie (1996), using bi-monthly averaged climatological hydrographic and surface wind-stress data.

Tidal currents account for about 80% of the current variation and kinetic energy over GB, with maximum M_2 currents on top of the bank exceeding 100 cm/s. Using a finite-element numerical model with 2–6 km resolution, Lynch and Naimie (1993) simulated the 3-D structure of the M_2 tide in the entire GOM/GB domain. They found that computed tidal currents generally were in good agreement with observations, with overall averaged ellipse deviations of about 6.1 and 4.7 cm/s for major and minor axes, and about 10° and 8° for phase and orientation. Their model experiments also showed that the ellipse deviations varied with horizontal resolution, about 17–50% larger for a coarser mesh than with a finer mesh.

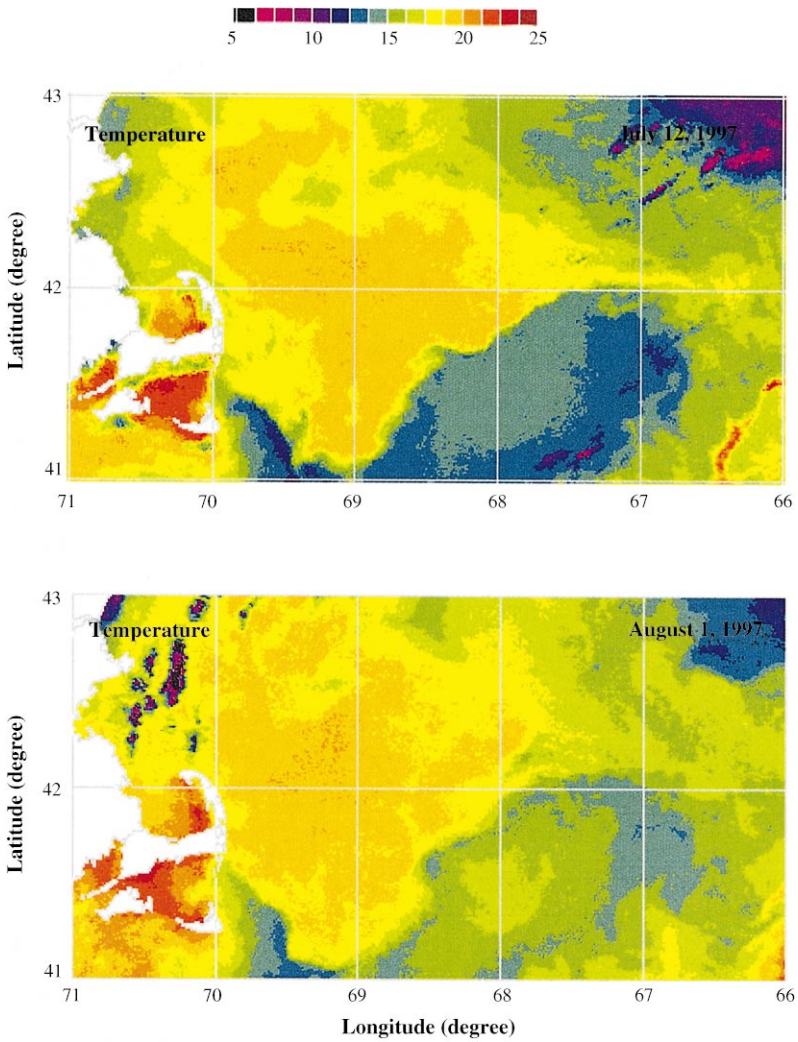

Fig. 3. Satellite images of sea-surface temperature on July 12 and August 1, 1997 in the Gulf of Maine and Georges Bank. These two figures were directly downloaded from the web site (http://rossby.sr.unh.edu/datasets/sst).

Summer satellite sea-surface temperature (SST) images generally revealed a relatively cold-water area within the tidal mixing frontal zones on GB and NS (Fig. 3). Loder and Greenberg (1986) showed that tidal mixing was sufficiently strong over the crest of GB to keep the local water column vertically well mixed throughout the year. Based on a tidally driven 2-D primitive equation model, Chen and Beardsley (1998) found that the tidal mixing varied spatially across GB. The cold-water band was thought to be formed by the spatial variation of tidal mixing related to local topography and bottom roughness acting on the ambient summer stratification.

Recently, Roworth and Signell (1998) complied a new high-resolution (15 s in latitude and longitude spacing, corresponding to roughly 0.4-km spacing) USGS bathymetric database for the GOM/GB domain. We used this new data set to configure our 3-D model, and then used this model to re-examine the influences of bottom topography on tidal simulation and the formation of residual circulation and tidal mixing fronts over Georges Bank. The rest of this paper describes the 3-D numerical model and experimental design, and results of tidal simulation, tidal mixing fronts, and 3-D residual circulation. The dynamics of tidal mixing are studied in Section 5. Effects of the irregular bottom topography and dynamical robustness of the 2-D model are discussed in Sections 6 and 7. A discussion of the cross-frontal secondary residual circulation is given in Sections 8 and 9.

2. The numerical model

The numerical model used in this study is the ECOM-si version of the 3-D coastal ocean circulation model developed originally by Blumberg and Mellor (1987). The model incorporates the Mellor and Yamada (1974, 1982) level 2.5 turbulent closure scheme as modified by Galperin et al. (1988) to provide a time and space-dependent parameterization of vertical turbulent mixing (MY2.5). This model uses the σ-coordinate in the vertical and curvilinear orthogonal coordinates in the horizontal. A semi-implicit scheme developed by Casulli (1990) is used for numerical computation, which treats the barotropic pressure gradient in the momentum equations and the velocity convergence in the continuity equation implicitly. The semi-implicit model is described in detail by Blumberg (1994), and a brief description is given below.

In an orthogonal curvilinear and σ-coordinate system, the primitive transport equations and equation of state are

$$\begin{aligned}&\frac{\partial(h_1h_2Du)}{\partial t}+\frac{\partial(h_2Du^2)}{\partial\xi_1}+\frac{\partial(h_1Duv)}{\partial\xi_2}+h_1h_2\frac{\partial(\omega u)}{\partial\sigma}+Dv\left[-v\frac{\partial h_2}{\partial\xi_1}+u\frac{\partial h_1}{\partial\xi_2}-h_1h_2f\right]\\&\quad=-gDh_2\frac{\partial\zeta}{\partial\xi_1}-\frac{gD^2h_2}{\rho_0}\int_\sigma^0\left[\frac{\partial\rho}{\partial\xi_1}-\frac{\sigma}{D}\frac{\partial D}{\partial\xi_1}\frac{\partial\rho}{\partial\sigma}\right]\mathrm{d}\sigma+\frac{h_1h_2}{D}\frac{\partial}{\partial\sigma}\left(K_m\frac{\partial u}{\partial\sigma}\right)+F_u,\end{aligned}\tag{1}$$

$$\begin{aligned}&\frac{\partial(h_1h_2Dv)}{\partial t}+\frac{\partial(h_2Duv)}{\partial\xi_1}+\frac{\partial(h_1Dv^2)}{\partial\xi_2}+h_1h_2\frac{\partial(\omega v)}{\partial\sigma}+Du\left[-u\frac{\partial h_1}{\partial\xi_2}+v\frac{\partial h_2}{\partial\xi_1}+h_1h_2f\right]\\&\quad=-gDh_1\frac{\partial\zeta}{\partial\xi_2}-\frac{gD^2h_1}{\rho_0}\int_\sigma^0\left[\frac{\partial\rho}{\partial\xi_2}-\frac{\sigma}{D}\frac{\partial D}{\partial\xi_2}\frac{\partial\rho}{\partial\sigma}\right]\mathrm{d}\sigma+\frac{h_1h_2}{D}\frac{\partial}{\partial\sigma}\left(K_m\frac{\partial v}{\partial\sigma}\right)+F_v,\end{aligned}\tag{2}$$

$$h_1 h_2 \frac{\partial \zeta}{\partial t} + \frac{\partial}{\partial \xi_1}\int_{-H}^{\zeta} (u h_2 D)\,\mathrm{d}z + \frac{\partial}{\partial \xi_2}\int_{-H}^{\zeta} (v h_1 D)\,\mathrm{d}z = 0, \tag{3}$$

$$\frac{\partial (h_1 h_2 D\theta)}{\partial t} + \frac{\partial (h_2 D u\theta)}{\partial \xi_1} + \frac{\partial (h_1 D v\theta)}{\partial \xi_2} + h_1 h_2 \frac{\partial (\omega\theta)}{\partial \sigma} = \frac{h_1 h_2}{D}\frac{\partial}{\partial \sigma}\left(K_h \frac{\partial \theta}{\partial \sigma}\right) + F_\theta \tag{4}$$

$$\rho_{\text{total}} = \rho_{\text{total}}(\theta, S_0) = \rho_0 + \rho, \tag{5}$$

where ξ_1 and ξ_2 are the horizontal curvilinear orthogonal coordinates; u, v, and ω are the ξ_1, ξ_2, and σ velocity components, θ the potential temperature, f the Coriolis parameter, g the gravitational acceleration, K_m the vertical eddy viscosity coefficient, K_h the thermal vertical eddy diffusivity, S_0 the reference salinity, ρ_0 the reference density, ρ the perturbation density, h_1 and h_2 the metric factors of the coordinate transformation on the ξ_1 and ξ_2 axes, and $D = \zeta + H$ the total water depth, where ζ and H are the surface elevation and reference depth from $z = 0$, respectively. F_u, F_v, and F_θ represent horizontal momentum and thermal diffusion terms. To simplify the model calculations, the reference salinity S_0 is kept constant so that density is solely a function of temperature.

The true vertical velocity w on a σ surface is calculated by

$$w = \omega - \frac{1}{h_1 h_2}\left[h_2 u\left(\sigma\frac{\partial D}{\partial \xi_1} + \frac{\partial \zeta}{\partial \xi_1}\right) + h_1 v\left(\sigma\frac{\partial D}{\partial \xi_2} + \frac{\partial \zeta}{\partial \xi_2}\right)\right] - \left(\sigma\frac{\partial D}{\partial t} + \frac{\partial \zeta}{\partial t}\right), \tag{6}$$

The vertical eddy viscosity and diffusion coefficients are calculated using the MY2.5 turbulent closure scheme, which includes (1) shear and buoyancy production of turbulent kinetic energy (TKE), (2) TKE dissipation, (3) TKE vertical diffusion, (4) TKE advection, and (5) temporal evolution of the TKE and turbulent macroscale. The 3-D equations for q^2 and $q^2 l$ are given by

$$\begin{aligned}&\frac{\partial (h_1 h_2 D q^2)}{\partial t} + \frac{\partial (h_2 D u q^2)}{\partial \xi_1} + \frac{\partial (h_1 D v q^2)}{\partial \xi_2} + h_1 h_2 \frac{\partial (\omega q^2)}{\partial \sigma}\\ &\quad = 2 h_1 h_2 D(P_s + P_b - \varepsilon) + \frac{h_1 h_2}{D}\frac{\partial}{\partial \sigma}\left(K_h \frac{\partial q^2}{\partial \sigma}\right) + F_{q^2},\end{aligned} \tag{7}$$

$$\begin{aligned}&\frac{\partial (h_1 h_2 D q^2 l)}{\partial t} + \frac{\partial (h_2 D u q^2 l)}{\partial \xi_1} + \frac{\partial (h_1 D v q^2 l)}{\partial \xi_2} + h_1 h_2 \frac{\partial (\omega q^2 l)}{\partial \sigma}\\ &\quad = 1.8 l h_1 h_2 D(P_s + P_b - 0.56\varepsilon \widehat{W}) + \frac{h_1 h_2}{D}\frac{\partial}{\partial \sigma}\left(K_h \frac{\partial q^2 l}{\partial \sigma}\right) + F_l,\end{aligned} \tag{8}$$

where $q^2 = (u'^2 + v'^2)/2$ is the turbulent kinetic energy, l the turbulent macroscale, K_q the vertical eddy diffusion coefficient of the turbulent kinetic energy, F_q and F_l represent the horizontal diffusion of the turbulent kinetic energy and macroscale, $P_s = K_m/D^2[(\partial u/\partial \sigma)^2 + (\partial v/\partial \sigma)^2]$, and $P_b = (gK_h/D\rho_s)(\partial \rho/\partial \sigma)$ the shear and buoyancy production terms of turbulent kinetic energy, $\varepsilon = 0.06 q^3/l$ the turbulent kinetic energy dissipation rate, $\widehat{W} = 1 + 1.33 l^2/(\kappa L)^2$ a wall proximity function, where $L^{-1} = (\zeta - z)^{-1} + (H + z)^{-1}$, $\kappa = 0.4$ the von Karman constant. In general, F_q and F_l are kept as small as possible to reduce the effects of horizontal diffusion on the solutions.

The turbulent kinetic energy and macroscale equations are closed by defining

$$K_m = lqS_m, \quad K_h = lqS_h, \quad K_q = 0.2lq. \tag{9}$$

S_m and $S_h$are defined as the stability functions

$$S_m = \frac{0.39 - 3.89G_h}{1 - 34.68G_h(1 - 10.1G_h)}, \quad \text{and} \quad S_h = \frac{0.49}{1 - 34.66G_h}, \tag{10}$$

where $G_h = (l^2 g/q^2\rho_0 D)(\partial\rho/\partial\sigma)$. In the original MY2.5 turbulent closure model (Mellor and Yamada, 1974, 1982), S_m and S_h are functions of the gradient Richardson number. By removing a slight inconsistency in the scaling analysis, Galperin et al. (1988) simplified the MY turbulent closure model so that S_m and $S_h$depend only on G_h. G_h has an upper bound of 0.023 for the case of unstable ($\rho_z > 0$)stratification and with a lower bound of -0.28 for the case of stable ($\rho_z < 0$) stratification.

The surface and bottom boundary conditions for momentum and heat are

$$\begin{aligned} &\frac{\rho_0 K_m}{D}\left(\frac{\partial u}{\partial\sigma}, \frac{\partial v}{\partial\sigma}\right) = (\tau_{ox}, \tau_{oy}), \quad \frac{\partial\theta}{\partial\sigma} = 0, \quad \omega = 0 \quad \text{at } \sigma = 0, \\ &\frac{\rho_0 K_m}{D}\left(\frac{\partial u}{\partial\sigma}, \frac{\partial v}{\partial\sigma}\right) = (\tau_{bx}, \tau_{by}), \quad \frac{\partial\theta}{\partial\sigma} = 0, \quad \omega = 0 \quad \text{at } \sigma = -1, \end{aligned} \tag{11}$$

where (τ_{ox}, τ_{oy}) and $(\tau_{bx}, \tau_{by}) = C_d\sqrt{u^2 + v^2}(u, v)$ are the ξ_1 and ξ_2 components of surface wind and bottom stresses. The surface wind stress is calculated based on the neutral steady-state drag coefficient developed by Large and Pond (1981). The bottom drag coefficient C_d is determined by matching a logarithmic bottom layer to the model at a height z_{ab} above the bottom, i.e.

$$C_d = \max\left[k^2/\ln\left(\frac{z_{ab}}{z_0}\right)^2, 0.0025\right], \tag{12}$$

where z_0 is the bottom roughness parameter, and z_{ab} is the height above the bottom of the first velocity (u, v) grid node.

The surface and bottom boundary conditions for the turbulent kinetic energy and macroscale equations are

$$q^2 l = 0, \quad q^2 = B_1^{2/3}u_{\tau s}^2 \text{ at } z = \zeta \quad \text{and } q^2 l = 0, \quad q^2 = B_1^{2/3}u_{\tau b}^2 \quad \text{at } z = -H, \tag{13}$$

where $u_{\tau s}$ and $u_{\tau b}$ are the friction velocities associated with the surface and bottom stresses, respectively, and B_1 an empirical constant equal to 16.6.

The value of z_0 is thought to vary widely within the GB/GOM domain, especially over the shallow top of Georges Bank where very large (up to 10-m high) sand waves exist and some areas are covered with gravel. The estimation of z_0 versus ratio of the orbital wave velocity to the current speed over GB varies in a wide range from 0.1 to 35 mm (Werner and Beardsley, 2000). Based on "law of the wall" log profile fits to near-bottom currents measured at ST1 (40°51.8′, 67°33.5′), Werner and Beardsley (2000) suggest that $z_0 = 0.6$ mm is a good estimate for the sandy mid-shelf region around the ST1 site on the southern flank of GB.

In previous model studies of GB, z_0 has varied widely. In Chen et al. (1995a), $z_0 = 1.0$ mm, and in Naimie (1996), C_d was specified as a constant value of 0.005 and $z_{ab} = 1$ m, which was equivalent to a setting of $z_0 = 3.5$ mm. In the updated version of the Princeton Ocean Model (POM), z_0 is taken as a function of water depth (D), such that z_0 increases as D decreases. We have chosen $z_0 = 0.6$ mm for our 3-D model experiments. To examine the sensitivity of tidal simulation to z_0, we also have conducted numerous experiments using a wide range of z_0 or z_0 as a function of depth.

The numerical domain covered the GOM/GB region and was enclosed by an open boundary running from the New Jersey shelf to the Nova Scotia shelf (Fig. 4). The orthogonal curvilinear coordinate system was chosen to give better horizontal resolution over the GOM/GB, varying from 1.5 to 3 km over GB and in the interior region of the GOM expanding to 4–20 km near the open boundary. Based on Chen et al. (1995a) and Haney (1991), uniform grid spacing was used in the vertical to reduce σ-errors over steep topography. Most experiments were conducted with 31 σ-levels, providing 1.3–4 m vertical resolution over the depth range 40–120 m on GB and 10-m spacing over the off-bank depth of 300 m. (Some experiments were repeated with 61 σ-levels, with little difference in the results.) The bottom depth at each model grid point was interpolated directly from the new USGS bathymetry database. The model time step was 414 s, which resulted in 108 time steps over a M_2 (12.42 h) tidal cycle.

The model was forced along the open boundary by the surface M_2 elevation and phase taken from the global $0.5^\circ \times 0.5^\circ$ inverse tidal model of Egbert et al. (1994). A gravity-wave radiation condition on current was applied at the open boundary to minimize energy reflection into the computational domain. To examine the influence of wind forcing during summer conditions, a mean northeastward wind of 3 m/s was used in the model experiments.

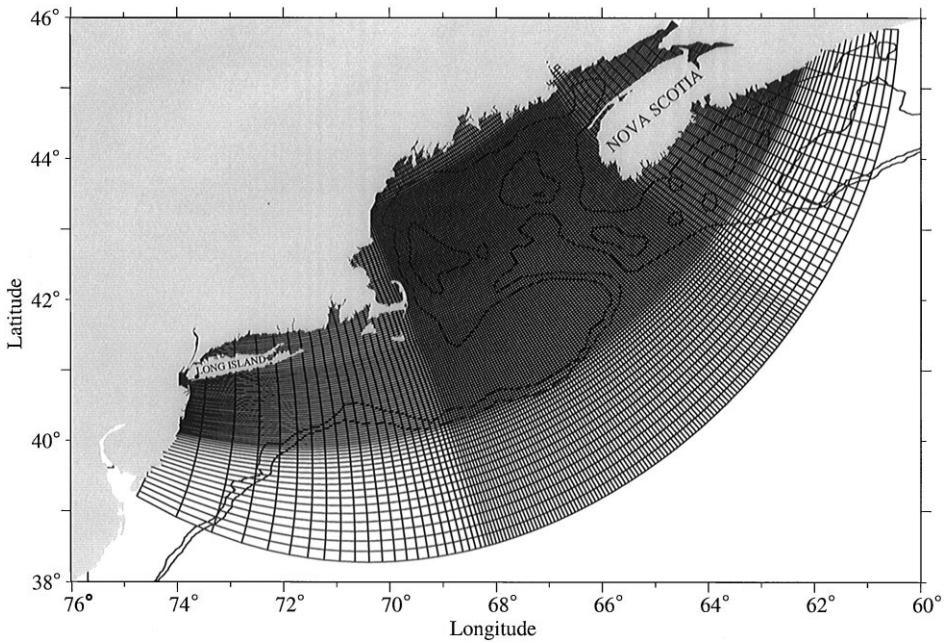

Fig. 4. The numerical model horizontal orthogonal curvilinear coordinate system.

To facilitate comparison with the 2-D model results presented by Chen et al. (1995a), we ran the 3-D model as an initial value problem with homogeneous and early summer stratification. The initial summer temperature distribution was specified by a linear function of z, with a value of 15°C at the surface and 6°C at a depth of 300 m. The resulting initial Brunt Väisälä frequency N for this case is $10^{-2}\,s^{-1}$, which is typical of early summer (late May or early June) stratification over GB.

3. The M_2 tidal simulation

To test the capability of our 3-D model for tidal simulation, we ran the model for homogeneous conditions with tidal forcing, and found the predicted currents over GB were especially sensitive to the choice of z_0. Forced directly by the global tidal elevation and phase along the open boundary, the model tended to overestimate the tidal elevation and current amplitudes over GB as z_0 was decreased. A good comparison between the model predicted and observed elevations and tidal currents was found for the case with $0.6\,mm \leqslant z_0 \leqslant 10\,mm$ {using a depth-dependent form of z_0 where $z_0 = 10\,mm$ as $D \leqslant 60\,m$ and $z_0 = 10[1 + (60 - D)/D]$ (mm)}. As we will see in Section 5, such large values of z_0 lead to significant overestimation of turbulent dissipation ε in the mixed region, exaggerating the strength of tidal mixing. Alternatively, we reduced the amplitude of the tidal forcing at the open boundary by about 10% and ran the model with the constant value $z_0 = 0.6\,mm$. The model then provided a reasonable simulation of tidal elevation and current as well as turbulent dissipation in the mixed region over GB. The model-data comparisons described below are based mainly on this adjusted experiment.

The computed tidal elevation and currents were compared directly with previous observations taken at stations shown in Fig. 5. The model predicted that the M_2 surface tide propagated into the GOM from the open ocean and turned clockwise to the northeast with an amplitude increase from 50 cm over GB to 300 cm or higher in the Bay of Fundy (Fig. 6). The tidal phase was almost parallel to the major axis of GB and then turned clockwise within the GOM. The model-predicted spatial distributions of co-amplitude and co-phase are in good agreement with observed co-tidal charts drawn by Moody et al. (1984). Detailed comparison between computed and observed amplitudes and phases is given in Table 1. The overall deviation at 38 tidal measurement stations was 3.6 cm in amplitude and 4.2° in phase. On GB, the difference at most stations ranged from 1 to 3 cm in amplitude and 0.4 to 5° in phase. Relatively large amplitude difference was found at stations 19, 25, and 30 (around the northwestern GOM coast). This is likely caused by low horizontal model resolution along the coast as suggested by Lynch and Naimie (1993).

Tidal currents exhibited a rotary character over GB, increasing northward across the bank, from a maximum velocity of 30 cm/s at the shelf break on the southern flank to about 100 cm/s at the crest. The model-predicted tidal current ellipses were in good agreement with observations at selected measurement stations over GB (Moody et al., 1984; Brown, 1984; Butman and Fry, 1990; Chen et al., 1995b; Werner and Beardsley, 1999) (Fig. 7 and Table 2). The overall deviation at 32 stations was 4.1 cm/s in major axis, 3.6 cm/s in minor axis, and 6.4° in orientation, which are around the maximum error bars of current measurements.

The vertical structure of the computed M_2 tidal current coincided well with observations at selected stations A (#25), K (#27), and P3 (#24) on the southern and northeastern flanks of GB (Fig. 8). When the depth-dependent form of z_0 was used with the unadjusted tidal forcing, the

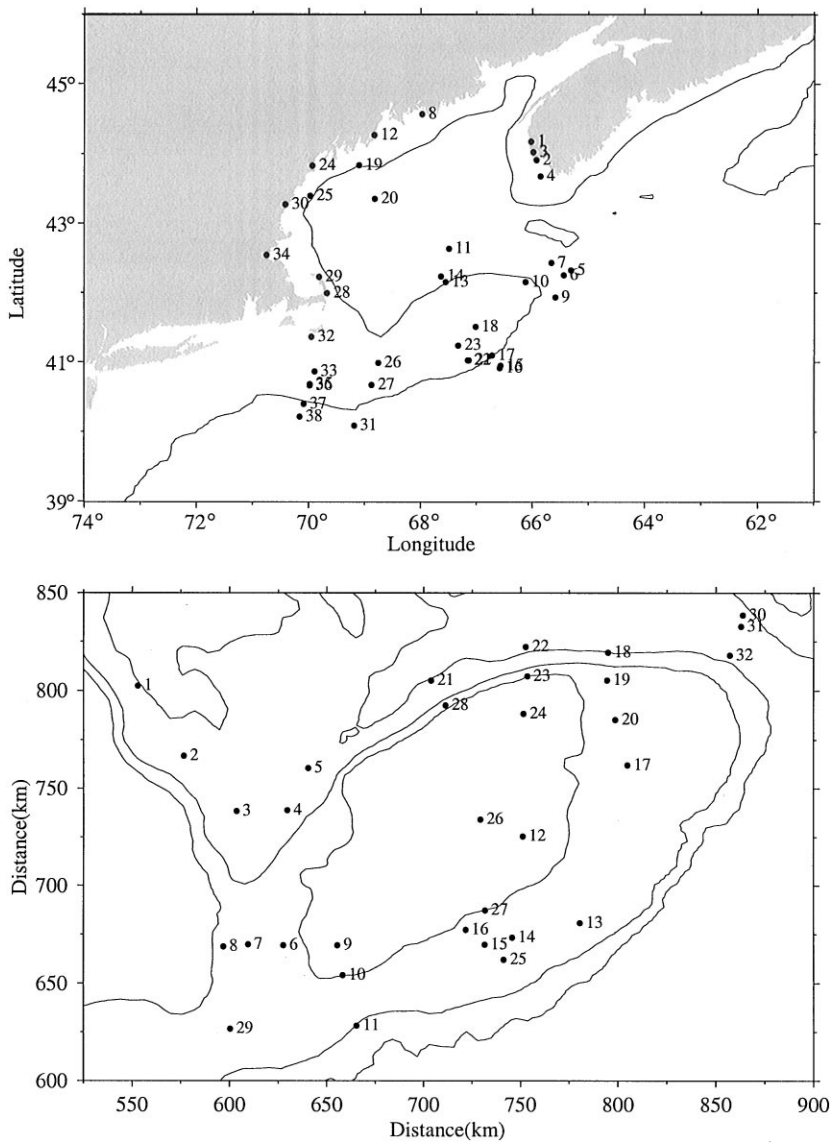

Fig. 5. Selected stations for the model-data comparison of tidal elevation (upper) and current (lower). The data sources used in the comparison include Moody et al. (1984), Butman and Fry (1990), Chen et al. (1995b), and Werner and Beardsley (1999).

model predicted increased vertical current shear at three stations where $z_0 = 7.1$ (A), 9.3 (K), and 10 (P3) mm, which showed a little better agreement with the observed current profiles.

Our 3-D model simulation of tidal elevation and currents over GB is generally consistent with previous model tidal predictions made by Greenberg (1983) and Lynch and Naimie (1993). However, like some other 3-D model studies, this model also failed to simulate closely the tidal amplitude in the Bay of Fundy, due in part to the coarsely resolved bottom topography used in that region.

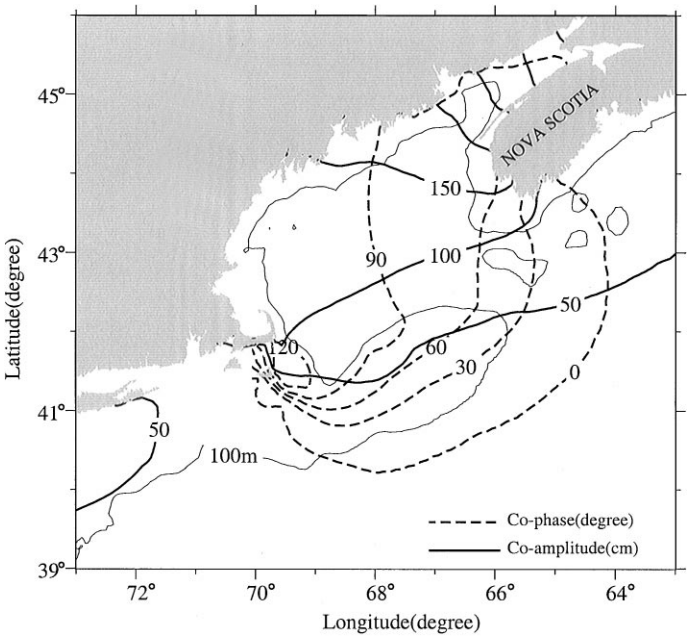

Fig. 6. The model-predicted co-tidal chart of the M_2 tidal elevation. Co-amplitude (cm) and co-phase (degree) lines are plotted every 50 cm and 30°, respectively.

We found that the tidal current simulation on Georges Bank was significantly improved when the high-resolution topography data were used, and that the results were sensitive to the value and spatial dependence of z_0. This is not an unexpected result, since tidal modelers have long used z_0 (or C_d) as a tunable parameter to obtain the best fit between observed and model tides. What is interesting here is the further influence of spatial variation of z_0 on the prediction of tidal dissipation and mixing.

4. Tidal mixing fronts and residual circulation

To examine how stratification and tidal mixing influence the clockwise residual circulation over GB and adjacent coastal regions of the GOM, we ran the model with the adjusted M_2 forcing for both homogeneous and early summer stratification cases. The residual currents were calculated by averaging over one tidal cycle after the tidal currents and temperature reach a quasi-equilibrium state (5 days for homogeneous case and 10 days for the stratification case).

4.1. Homogenous case

With no stratification, the model predicted a topographically controlled clockwise residual circulation around GB and Browns Bank (BB) and a strong southward residual current over NS (Fig. 9). Over GB, the water flowed eastward to southeastward as a strong jet with a maximum

Table 1
Comparison of observed and computed M_2 tidal elevations at reference sites[a]

Site	Amplitude (m)			Phase (°G)		
	ζ_0	ζ_c	$\Delta\zeta$	ϕ_0	ϕ_c	$\Delta\phi$
1	185.9	185.1	0.8	67.1	66.0	1.1
2	159.1	155.4	3.7	56.4	59.0	− 2.6
3	168.2	163.2	5.0	62.2	63.0	− 0.8
4	125.0	120.4	4.6	47.0	52.0	− 5.0
5	44.0	45.8	− 1.8	10.2	4.0	6.2
6	44.0	44.2	− 0.2	15.5	9.0	6.5
7	50.4	45.2	5.2	27.9	24.0	3.9
8	159.1	154.9	4.2	87.4	93.0	− 5.6
9	38.7	39.6	− 0.9	5.3	2.0	3.3
10	45.6	41.0	4.6	37.6	38.0	− 0.4
11	91.9	88.3	3.6	85.0	87.0	− 2.0
12	151.2	150.0	1.2	95.1	98.0	− 2.9
13	78.7	75.8	2.9	98.5	93.0	− 3.5
14	83.0	78.2	4.8	90.7	92.0	− 1.3
15	37.0	40.5	− 3.5	2.4	356.0	6.4
16	37.1	40.5	− 3.4	2.3	355.0	7.3
17	37.3	38.9	− 1.6	6.3	1.0	5.3
18	39.4	39.6	− 0.2	25.1	22.0	3.1
19	136.4	130.3	6.1	95.8	99.0	− 3.2
20	125.5	120.0	5.5	96.4	98.0	− 1.6
21	38.0	38.9	− 0.9	11.3	6.0	5.3
22	38.0	38.9	− 0.9	11.3	5.0	6.3
23	39.8	39.9	− 0.1	23.2	18.0	5.2
24	138.9	133.0	5.9	100.3	103.0	− 2.7
25	133.5	127.2	6.3	101.8	103.0	− 1.2
26	26.1	25.9	0.2	48.9	47.0	1.9
27	31.5	31.4	0.1	8.7	3.0	5.7
28	108.6	103.2	5.4	111.5	102.0	9.5
29	119.1	116.0	3.1	108.8	113.0	− 4.2
30	137.9	130.3	7.6	103.2	107.0	− 3.8
31	38.4	41.9	− 3.5	355.2	349.0	6.2
32	31.0	32.3	− 1.3	1.5	1.0	0.5
33	38.7	38.7	0.0	358.0	356.0	2.0
34	139.0	134.5	4.5	106.4	111.0	− 4.6
35	40.8	38.7	2.1	355.4	353.0	2.4
36	39.6	40.4	− 0.8	356.3	354.0	2.3
37	41.5	42.0	− 0.5	353.9	353.0	0.9
38	42.0	41.9	0.1	353.7	351.0	2.7
Overall deviation			3.6			4.2

[a] ζ_0 and ϕ_0 are the observed amplitude and phase, and ζ_c and ϕ_c are the computed amplitude and phase.

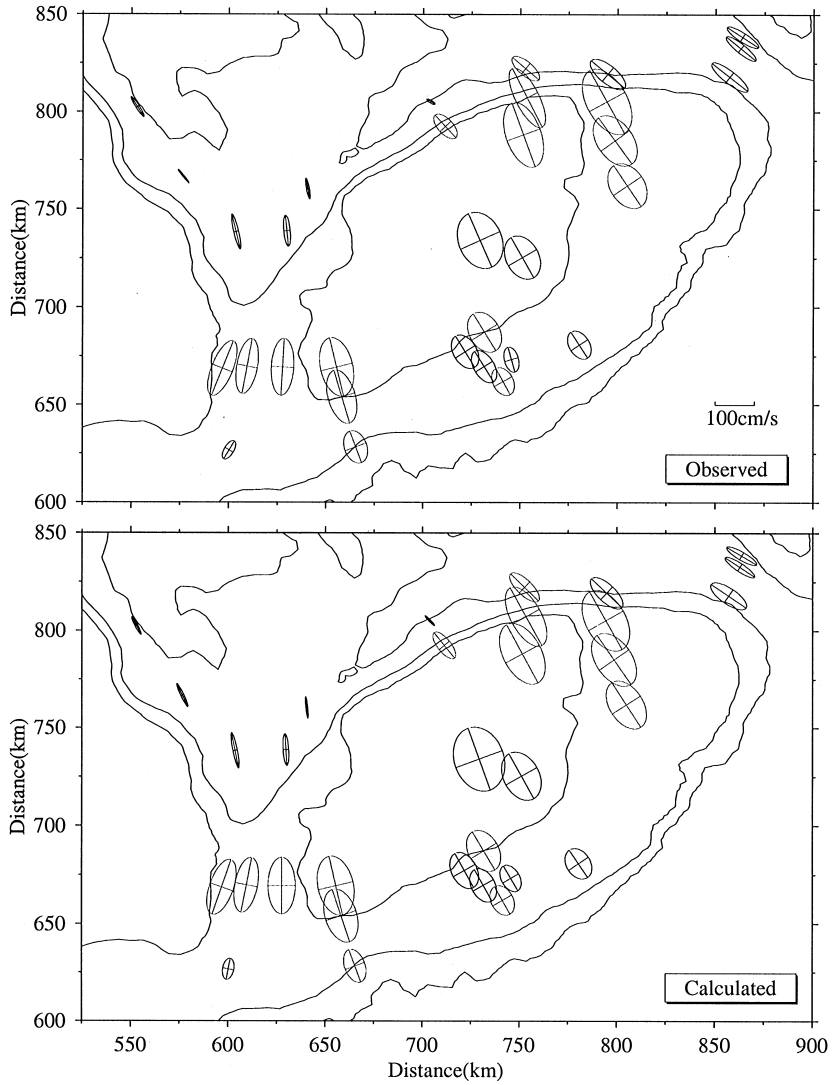

Fig. 7. Comparison between measured and computed M_2 tidal currents at selected tidal stations over GB, GSC, and the NEC. The measurement depth of the tidal current is listed in Table 2.

speed of about 14–16 cm/s along the northern flank, then flowed to the southern flank along two main paths between the 40 to 60 m isobaths and along the 100-m isobath as relatively weak and broader flows with maximum speeds of about 3–5 cm/s. These weak flows then turn back (recirculate) to the northwest and northern flanks mainly along the 40–60-m isobaths. The residual current was surface-intensified, and significant upwelling of about 0.01 cm/s was found on the slope of the northern flank.

Unlike the cases with smoothed bottom topography shown in previous model efforts (e.g., Greenberg, 1983; Naimie, 1996), the model predicted several small-scale clockwise circulation

Table 2
Comparison of computed and observed M_2 tidal ellipse parameters[a]

Site	Instr. depth (m)	$\hat{U}_{major}$ (cm/s)	U_{major} (cm/s)	ΔU (cm/s)	$\hat{U}_{minor}$ (cm/s)	U_{minor} (cm/s)	ΔU (cm/s)	$\hat{\phi}_{orien}$ (deg-G)	ϕ_{orien} (deg-G)	$\Delta\phi$ (deg-G)
1	Averaged	25.8	30.5 ± 1.1	− 4.7	3.6	4.4 ± 0.7	− 0.8	118.4	122.8 ± 0.8	− 4.4
2	Averaged	33.0	21.9 ± 0.8	11.1	4.0	1.9 ± 0.3	2.1	115.6	129.2 ± 0.8	− 13.6
3	Averaged	46.0	45.4 ± 1.6	0.6	− 5.5	− 6.0 ± 1.0	0.5	101.4	103.5 ± 0.9	− 2.1
4	Averaged	40.5	39.4 ± 1.4	1.1	− 7.0	− 8.2 ± 1.4	1.2	93.6	95.7 ± 1.0	− 2.1
5	Averaged	27.6	26.5 ± 0.9	1.1	− 2.7	− 3.9 ± 0.6	1.2	95.6	100.6 ± 1.0	− 5.0
6	10	72.3	73.2 ± 3.1	− 0.9	− 35.2	− 28.9 ± 1.8	− 6.3	90.0	86.7 ± 2.0	3.3
7	10	71.2	71.5	− 0.3	− 29.1	− 26.6	− 2.5	78.9	79.8	− 0.9
8	10	73.7	75.4	− 1.7	− 30.6	− 27.1	− 3.5	70.7	68.1	2.6
9	10	76.8	76.5	0.3	− 45.7	− 41.6	− 4.1	103.0	103.7	− 0.7
10	10	70.5	70.5	0.0	− 40.4	− 35.0	− 5.4	108.7	106.6	2.1
11	10	44.3	43.1	1.2	− 26.3	− 28.8	2.5	110.3	110.7	− 0.4
12	36	65.6	58.8 ± 1.0	6.8	− 45.7	− 41.9 ± 0.9	− 3.8	119.2	120.0	− 0.8
13	10	42.0	39.5 ± 2.2	2.5	− 30.6	− 25.9 ± 2.0	− 4.7	124.1	123.0	1.1
14	71	36.7	33.0 ± 1.4	3.7	− 23.5	− 18.1 ± 1.1	− 5.4	120.6	106.0	14.6
15	Averaged	46.0	46.0	0.0	− 30.3	− 26.0	− 4.3	119.2	122.0	− 2.8
16	Averaged	49.5	47.0	2.5	− 32.4	− 30.0	− 2.4	119.1	122.0	− 2.9
17	15	68.4	63.1 ± 1.4	5.3	− 42.6	− 43.5 ± 0.7	0.9	123.0	124.0 ± 1	− 1.0
18	79	53.7	55.5	− 1.8	− 22.4	− 22.7	0.3	136.7	141.0	− 4.3
19	19	84.8	91.9	− 7.1	− 51.2	− 51.9	0.7	119.5	119.0	0.5
20	36	76.4	73.2 ± 0.3	3.2	− 46.1	− 45.5 ± 0.4	− 0.6	124.8	126.0 ± 3	− 1.2
21	77	17.7	12.5	5.2	− 2.6	− 3.6	1.0	134.8	149.0	− 14.2
22	75	49.9	44.3	5.6	− 19.4	− 17.7	− 1.7	136.3	140.0	− 3.7
23	30	84.6	84.8 ± 2.1	− 0.3	− 39.2	− 30.0 ± 0.7	− 9.2	119.1	117.0 ± 5	2.1
24	30	84.7	87.1	− 2.4	− 49.0	− 44.9	− 4.1	118.4	110.0	8.4
25	45	40.4	38.3 ± 1.6	2.1	− 28.3	− 26.0 ± 1.6	− 2.3	119.5	119.0 ± 3	0.5
26	15	84.0	74.3 ± 0.4	9.7	− 63.8	− 55.6 ± 1.2	− 8.2	110.1	114.0 ± 1	− 3.9
27	10	56.4	55.1	1.3	− 38.6	− 38.7	0.1	121.1	122.0	− 0.9
28	15	41.9	39.5 ± 3.1	2.4	− 17.1	− 19.3 ± 2.3	2.2	129.1	133.0 ± 5	− 3.9
29	79	27.4	26.7 ± 0.6	0.7	− 14.4	− 12.2 ± 0.8	− 2.2	78.9	59.0 ± 5	19.9
30	207	44.1	47.8 ± 0.8	− 3.7	− 10.3	− 11.4 ± 1.8	1.1	149.9	143.0 ± 4	6.9
31	106	45.0	48.6 ± 0.1	− 3.6	− 10.4	− 11.6 ± 1.4	1.2	146.5	141.0 ± 2	5.5
32	112	53.9	57.9 ± 2.9	− 4.0	− 20.1	− 15.5 ± 3.9	− 4.6	146.0	142.0 ± 0	4.0
Overall deviation					4.1		3.6			6.3

[a] $\hat{U}_{major}$, $\hat{U}_{minor}$, and $\hat{\phi}_{orien}$ are the computed major and minor axes, and orientation.

gyres over the top of GB within the 60-m isobath as a result of the locally varying topography. This residual circulation pattern also was much more complicated than that predicted by Lynch and Naimie (1993) in a case with 2–3 km resolution and un-smoothed bottom topography.

A closed clockwise residual circulation was also found over BB, but the current was much weaker (less than 5 cm/s). Over NS, the residual current flowed southward and then westward along the local topography. The maximum speed of this current was about 10 cm/s.

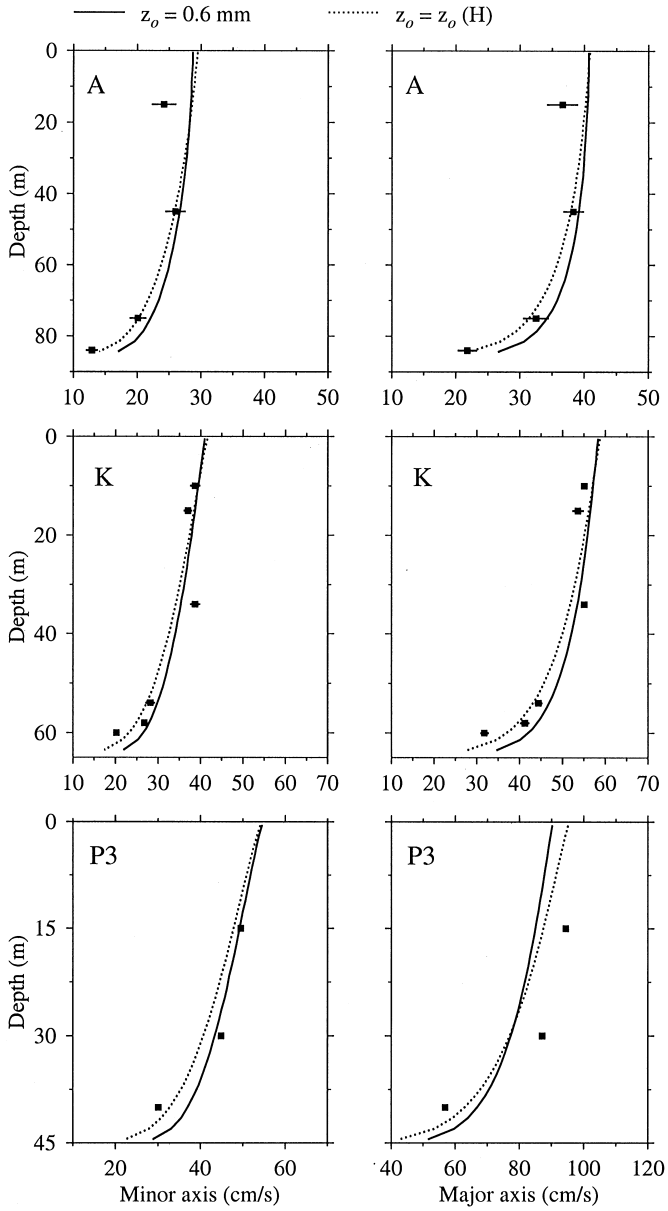

Fig. 8. Comparison between measured and computed amplitudes of tidal currents at stations numbered 25 (A), 27 (K), and 24 (P3) (Fig. 5). The solid and dashed lines present the model tidal current amplitude for the cases with $z_0 = 0.6$ mm everywhere and $z_0 = z_0(D)$. The filled squares indicate individual tidal current values at each station.

4.2. Stratified case

When early summer stratification was included, tidal mixing created well-defined tidal mixing fronts around GB, BB, and over NS (Fig. 10a). Over GB, the front was characterized by a narrow

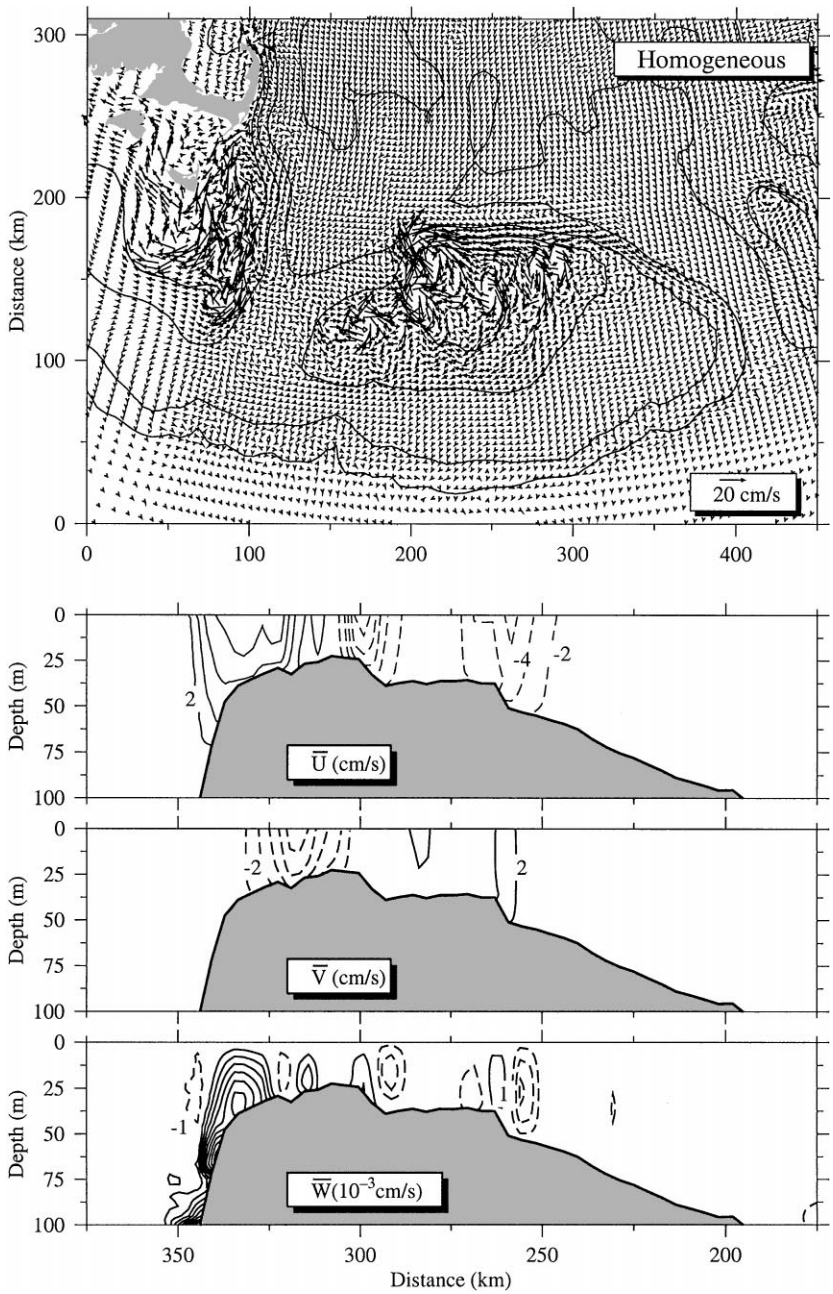

Fig. 9. Model-predicted surface vector field of residual currents (upper panel), and cross-bank distribution of along-bank (u), cross-bank (v), and vertical (w) residual current components along the cross-bank section 1 (shown in Fig. 1) for the homogeneous case. The contour intervals of the residual current are 2 cm/s for u and v and 1×10^{-3} cm/s for w.

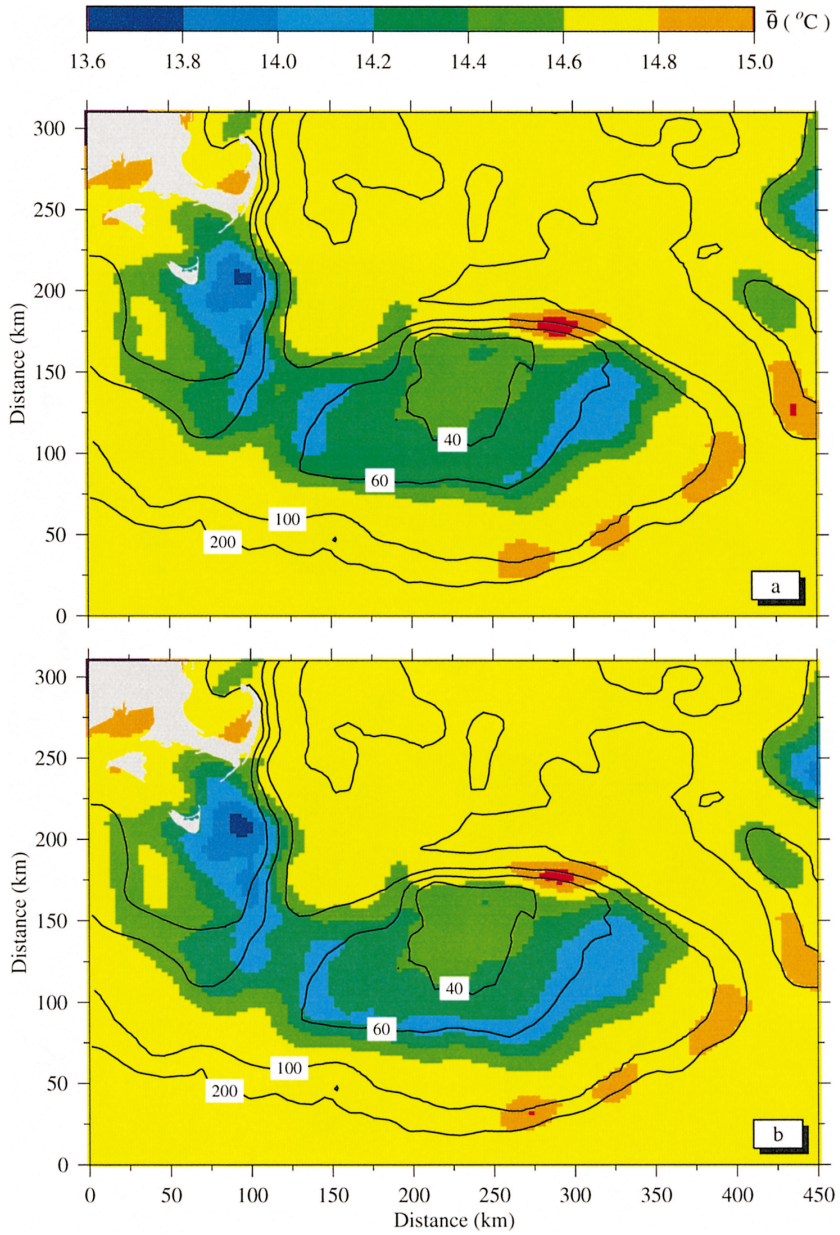

Fig. 10. Maps of tidally averaged surface temperature ($\bar{\theta}$ in °C) over Georges Bank and adjacent regions for the cases with (a) only tidal forcing and (b) tidal plus wind forcing.

zone at the 40-m isobath on the northern flank and a relatively wider region between the 50 and 60-m isobaths on the southern flank. Over NS, the water was vertically well mixed over the shallower region around Martha's Vineyard. A well-defined front was located along the 60-m isobath, which connected to GB across the GSC. The frontal zone on the southern flank of GB was

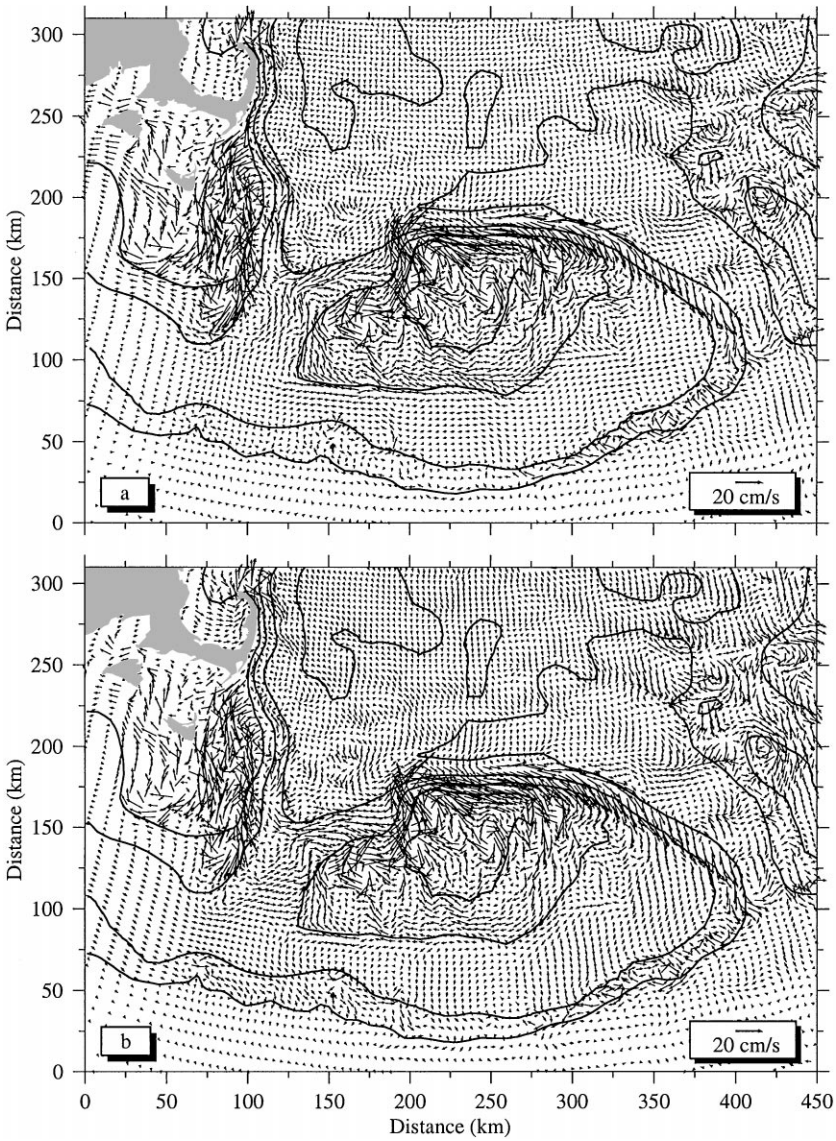

Fig. 11. Maps of tidally averaged near-surface residual current vectors over Georges Bank and adjacent regions for the cases with (a) only tidal forcing and (b) tidal plus wind forcing.

characterized by a relatively cold water band, with a minimum temperature on the eastern side of the bank. A similar cold water zone was found on NS through the GSC, which is consistent with the summertime SST images shown in Fig. 3. The existence of relatively cold water regions is due to vertical tidal mixing. Strong M_2 tidal currents tend to mix the local water column in the region shallower than 60 m over GB. Since tidal mixing starts at the bottom and grows upward locally, the vertically well-mixed water should be colder in a deeper region than at the crest during summer.

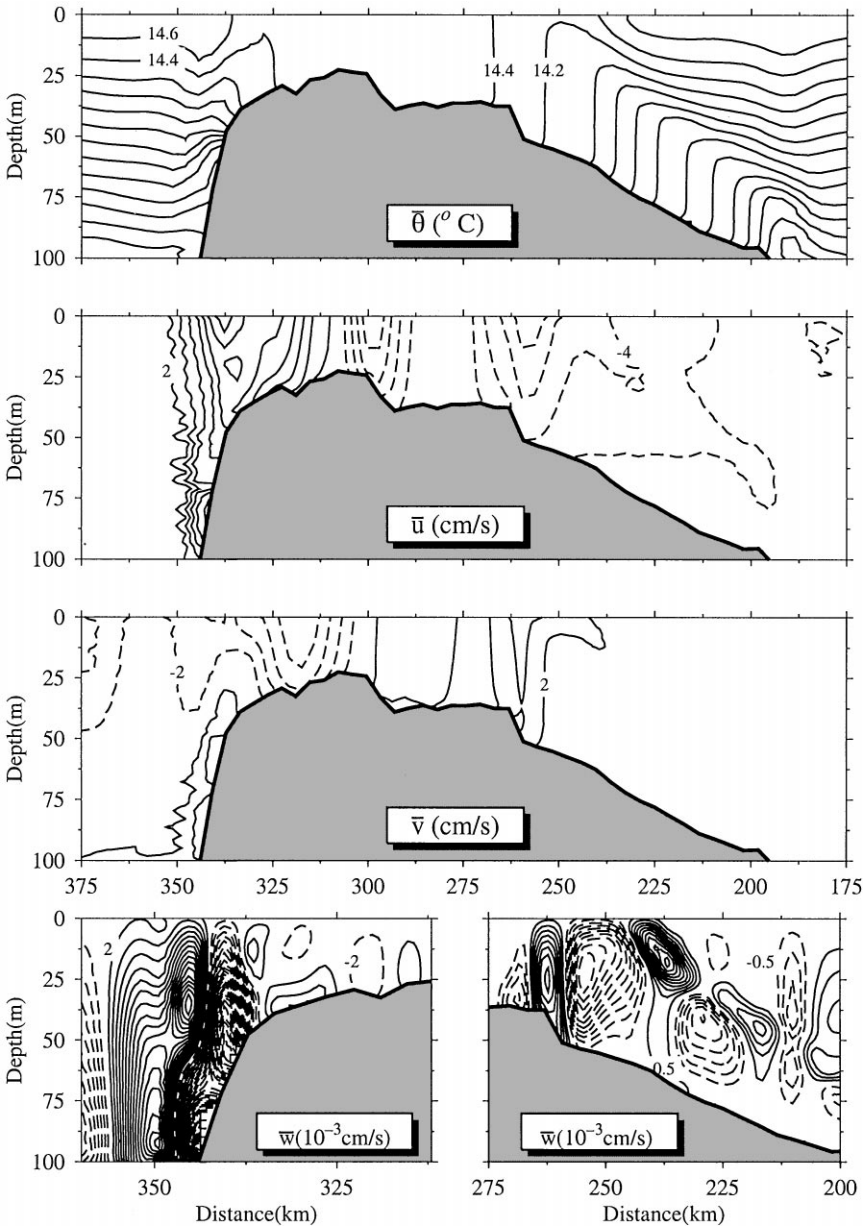

Fig. 12. Cross-bank distribution of the tidally averaged temperature ($\bar{\theta}$), eastward ($\bar{u}$), northward ($\bar{v}$), and vertical current ($\bar{w}$) on section 1 (shown in Fig. 1) for the case with only tidal forcing. The contour interval is 0.2°C for $\bar{\theta}$, 2 cm/s for $\bar{u}$ and $\bar{v}$, and 2×10^{-3} cm/s on the northern flank and 0.5×10^{-3} cm/s on the southern flank for $\bar{w}$.

The formation of tidal mixing fronts significantly enhanced the residual current within the frontal zones. Over GB, the along-bank current increased to 28–30 cm/s on the northwestern flank, 20–25 cm/s on the northern flank, and 5–8 cm/s on the southern flank (Figs. 11a and 12). The model predicted three main re-circulating paths of stratified residual flow on the northeastern part of GB:

(1) along the 40-m isobath, (2) between the 40 and 60-m isobaths, and (3) along the 100-m isobath. Small-scale clockwise residual flows in the region shallower than 60 m on the top of GB also became much stronger compared with those in the homogeneous case. Also, several small-scale eddy-like residual flows were found at the southern shelf break, which led to the formation of isolated warm cores at the outer edge of GB (Figs. 10a). Over NS, the southward residual current increased to 10–15 cm/s on the southwest flank of Cape Cod. A significant on-shelf component of residual flow was found on the eastern NS shelf, which may be due to the local irregular topography. The northward direction of the model-predicted current along the western shelf side of the GSC is in the opposite direction in comparison to ADCP current measurements (Chen et al., 1995b). This is likely due to the lack of a low-salinity surface plume in our numerical experiments which normally forms each spring as a result of local river runoff into the GOM and the around-Gulf flow of low-salinity water from the Scotian Shelf.

The model predicted residual circulation patterns over GB and NS were consistent qualitatively with the summertime drifter trajectories found by L&B and quantitatively with ADCP current measurements reported by Chen et al. (1995b). Both model and drifter data showed a narrow current zone on the northern flanks and three relatively strong re-circulation paths on the eastern side of GB. Small-scale drifter experiments, conducted on the southern flank during late spring of 1995 and 1997 by Churchill and Manning (1997) (C&M) show that their drifters tended to converge toward the southern tidal front at speeds up to 8 cm/s. This kind of on-bank convergent flow was evident in our 3-D model results, although it was a little weaker than the observed drifter velocities. Both drifter and moored current meter data show a strong jet current of about 30–40 cm/s on the northern flank, which was about 5–10 cm/s larger than the model-predicted value here. This difference may be due to the lack of seasonal heating in the model, which will be discussed in detail in a later paper by Chen et al. (2000).

Model-predicted cross-frontal secondary circulation varied with the slope of the bottom topography over GB (Fig. 12). On the northern flank, a bottom-intensified double cell flow occurred, with a front-ward convergence near the surface and a divergence near the bottom. The maximum vertical residual velocity was about 0.03 cm/s in the downwelling and upwelling regions. The center of the near-surface convergence was located at the axis of the maximum along-bank residual current within the front. On the southern flank, the cross-frontal secondary circulation was characterized by an asymmetric double cell circulation, with a divergence at the edge of the front near the surface and a convergence at the top of the bottom mixed layer. Two branches of upwelling were noticeable within the southern frontal zone: one was along isopycnals at the top of the bottom mixed layer and another was along in the lower part of the on-bank edge of the front. These two upwelled waters merged near the surface at the edge of the front, causing a maximum upward vertical velocity of 0.006 cm/s at a depth of about 15 m below the surface. In addition, the cross-bank secondary current above and below the bottom mixing layer in the stratified region over the southern flank was characterized by multiple circulation cells. These cells were stronger at the shelf break where the bottom was steep and become weaker as the thickness of the bottom mixing layer increases due to strong mixing. A clockwise circulation cell also was noticed within the relatively cold zone between the 38 and 52 m isobaths. It is a result of the local variable bottom topography, because it disappeared in the case with smoothed topography, which eliminated such local variations.

4.3. Wind effects

A northeastward wind of 3 m/s was applied on the model after the equilibrium residual flow state was reached. Over GB, this wind forcing reduced the near-surface, on-bank convergence current along the 60-m isobath on the southern flank and enhanced the eastward current on the northeastern flank near the GSC (Figs. 11b and 13). Although no significant change in the magnitude of along-bank residual current was found on the southern flank of GB and over NS (Figs. 10 and 11), the vertical temperature structure within the frontal zones was modified due to wind mixing. The water around the 60-m isobath on the southeastern side of GB and over NS was about 0.1°C colder than in the case of tidal forcing only. This cooling was caused by both surface wind mixing and wind-induced upwelling along the isopycnals above the bottom mixed layer.

4.4. The northeastern flank

The northeastern flank was characterized by stronger tidal mixing due to the steeper bottom slope and stronger tidal currents. This is an area connecting with the NEC where low-salinity water intrusions from the Scotian Shelf/Browns Bank area have been observed (Bisagni et al., 1996). In our 3-D model with simple forcing, the residual along-bank current split. On the cross-isobath transect near the splitting point, the model predicted a sub-surface intensified, along-bank residual current and relatively strong on-bank convergent flow at the tidal mixing front (Fig. 14a). Strong upwelling was found at the axis of the along-bank current jet, with a maximum just below the core of the current jet. The cross-isobath secondary circulation was characterized by a double-cell flow, with divergence at the axis of the along-bank current jet and convergence on both sides of the jet at the surface. Near the bottom of the slope, the current was dominated by relatively strong downwelling, with a maximum of 0.03 cm/s at a depth of about 125 m. This cross-isobath circulation pattern is significantly different from those on the southern and northern flanks shown in Figs. 12 and 13, and was little modified by the summertime mean wind (Fig. 14b).

4.5. Comparison between model and empirical-predicted tidal fronts

Simpson and Hunter (1974) examined the physical mechanisms responsible for tidal mixing and the formation of tidal mixing fronts, and found that tidal mixing was proportional to the parameter h/U^3 or $\log_{10}(h/D_t)$ where h is the local water depth, U a typical tidal current amplitude, and D_t the tidal kinetic energy dissipation rate ($D_t = \rho C_d U^3$ where C_d is the drag coefficient). Loder and Greenberg (1986) presented a map of $\log_{10}(h/D_t)$ for the GOM based on a 2-D (vertically averaged) tidal numerical model and the vertical density difference based on hydrography. They found that the location of the tidal mixing front (as defined by a difference in sigma-$t < 0.5$ over the top 50 m) coincided well with the $\log_{10}(h/D_t) = 1.9$ contour over Georges Bank and adjacent coastal regions. Chen et al. (1995c) compared the location of the tidal mixing front predicted by satellite SST images, hydrographic data, and $\log_{10}(h/D_t)$, and found that the observed tidal mixing front was in better agreement with the 2.1 contour than the 1.9 contour in the GSC, where a continuous frontal zone was found along the shallow sill across the GSC.

We also used the 3-D model output and topography to calculate $\log_{10}(h/D_t)$ for comparison with the location of the tidal mixing front predicted by our model for early summer stratification.

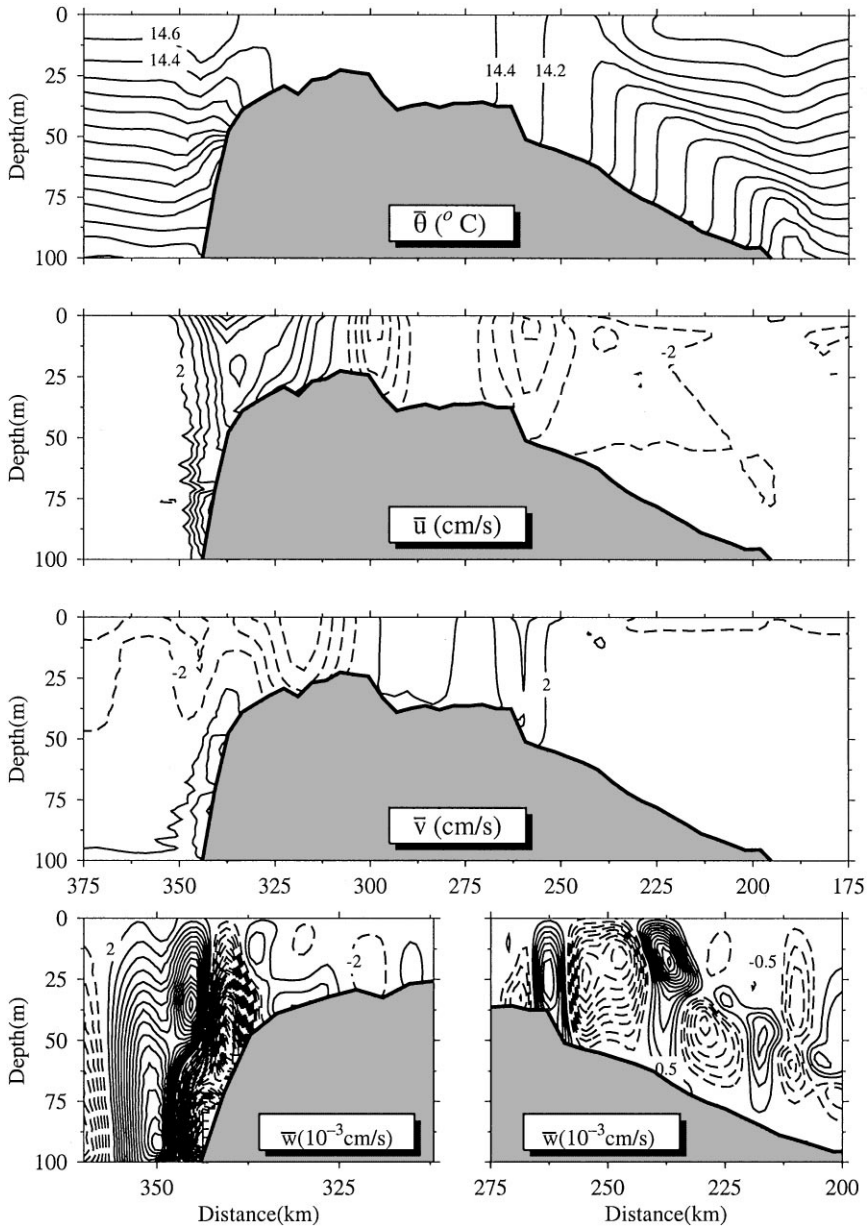

Fig. 13. Cross-bank distribution of tidally averaged temperature ($\bar{\theta}$), eastward ($\bar{u}$), northward ($\bar{v}$), and vertical current ($\bar{w}$) on section 1 for the case with tidal plus wind forcing. The contour intervals are the same as in Fig 12.

Good agreement was found between the location of the tidal mixing front and $\log_{10}(h/D_t) = 2.1$ over the outer banks (GB, NS, BB), and the Nova Scotia shelf off Cape Sable (Fig. 15). It should be pointed out here that the present model did not include other semidiurnal tidal constituents (such as S_2, N_2, and K_2, etc). These tidal components generally accounted for 10–20% of total tidal

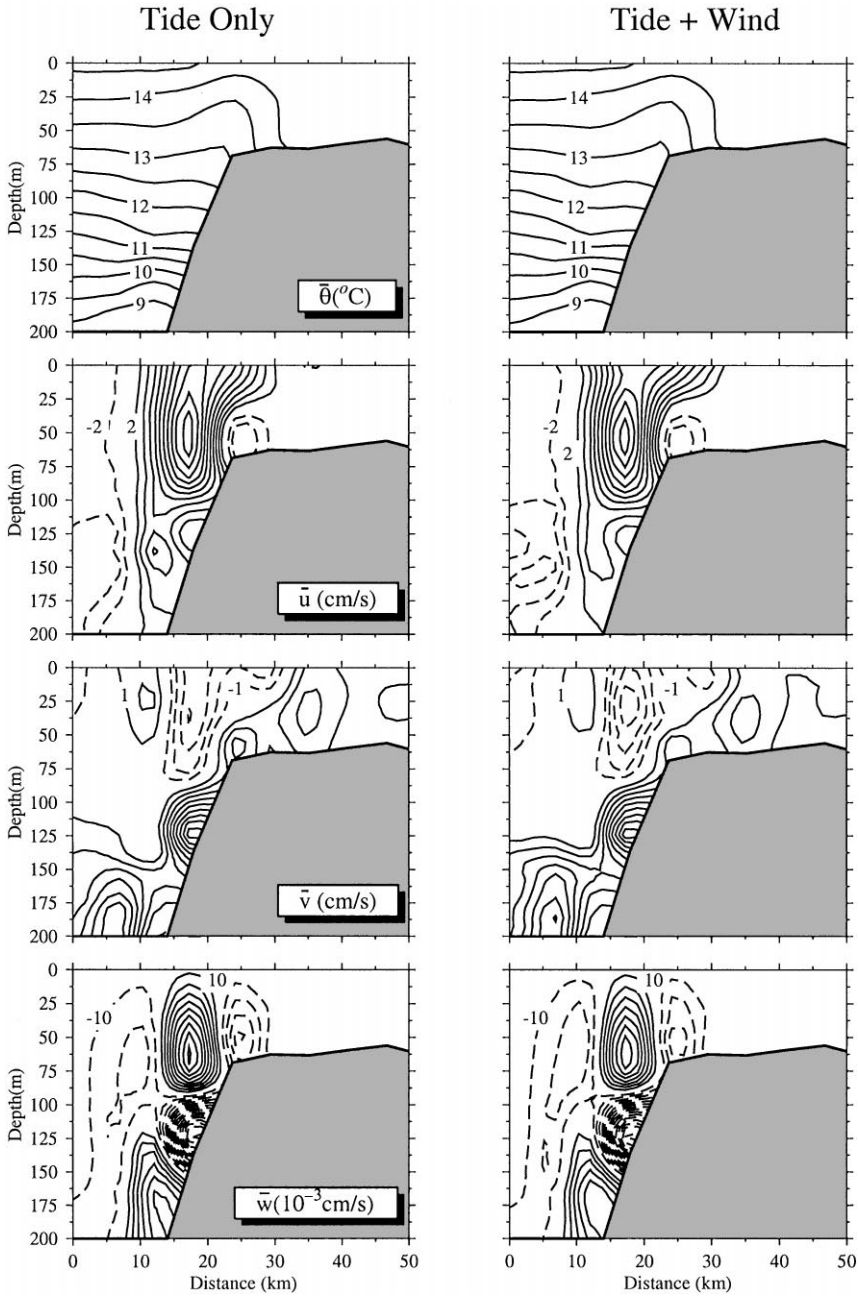

Fig. 14. Cross-bank distribution of tidally averaged temperature ($\bar{\theta}$), cross-section ($\bar{u}$), along-section ($\bar{v}$), and vertical current ($\bar{w}$) on section 2 (shown in Fig. 1) for the cases with tidal forcing only (left column) and tidal plus wind forcing (right column). The contour interval is 0.2°C for $\bar{\theta}$, 2 cm/s for cross-section flow, 1 cm/s for along-section flow, and 10×10^{-3} cm/s for $\bar{w}$.

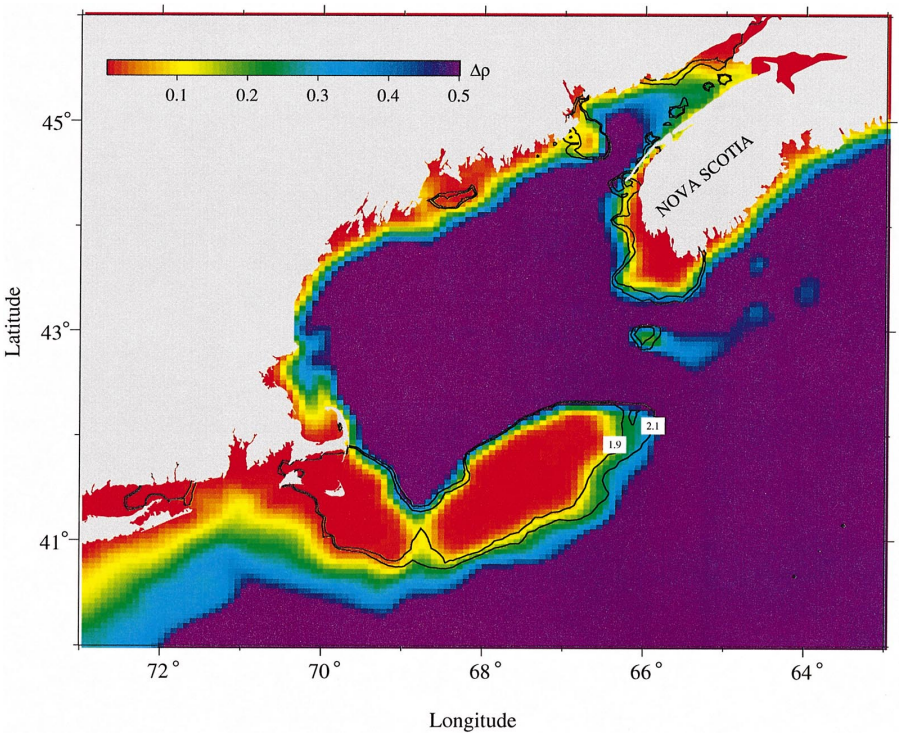

Fig. 15. Comparison of the tidal frontal locations predicted by our model and $\log_{10}(h/D_t)$. The color code indicates the model-predicted surface and bottom density difference for early summer stratification. The solid lines are the contours of $\log_{10}(h/D_t) = 1.9$ and 2.1.

dissipation D_t. Therefore, the location of the tidal mixing front could vary within $\log_{10}(h/D_t) = 1.9$ and 2.1 from spring to neap tidal cycles.

5. Tidal mixing

Vertical mixing in our model was computed using the MY2.5 turbulent closure model. In this model, the vertical eddy viscosity K_m is determined by the product of the turbulent kinetic energy q, the turbulent macroscale l, and the stability function S_m. q and l are functions of the magnitude of vertical shear of the horizontal current and vertical gradient of density, while S_m depends on the vertical density gradient. Physical processes that control the temporal and spatial variations of q and l include (1) the shear production of turbulence (P_s); (2) the buoyancy production of turbulence (P_b); (3) dissipation (ε); (4) advection; and (5) vertical diffusion.

5.1. Vertical eddy viscosity

The model showed that tidal mixing varied periodically with the magnitude and direction of the cross-bank tidal current (Fig. 16). At site C1 on the southern flank, where the water was stratified,

strong tidal mixing occurred only in the bottom boundary layer, a 25–30 m thick layer above the bottom. The vertical eddy viscosity K_m varied asymmetrically with tidal current, larger during the on-bank tidal flow as the colder water was advected upslope than during the off-bank tidal flow as the warmer water was pushed downslope. The maximum K_m was about $0.06\,m^2/s$, occurring at a middle depth of the bottom boundary layer after maximum on-bank tidal flow. At site C2 on top of the bank, where the water was vertically well mixed, K_m was characterized by a parabolic curve in the vertical, with a maximum at a depth of 15 m above the bottom, just a little lower than the middle water depth. K_m also varied in magnitude with the magnitude and direction of the tidal current, with a maximum value of about $0.06\,m^2/s$ during the on-bank flow and about $0.05\,m^2/s$ during the off-bank flow.

At site C3 on the northern flank, tidal mixing exhibited a much more complex time-dependent pattern. The cross-bank tidal current was asymmetrical in time. The maximum current occurred at a depth of about 20 m during the on-bank flow, but in a layer of about 30–50 m during the off-bank flow. The off-bank flow acted like a waterfall to advect warmer water down-slope with a displacement of 50 m, resulting in a relatively sharp thermal depression at the edge of the northern flank after maximum off-bank flow. Correspondingly, the resulting K_m was large, with a maximum of about $0.01\,m^2/s$ at a depth of 10 m below the surface. The temporal variation of K_m at the bottom was very similar to that found on the southern flank, larger during the on-bank flow as the colder water was advected up-slope than during the off-bank flow as the warmer water was pushed down-slope. The maximum value of K_m was about $0.04\,m^2/s$, occurring about 2 h after the maximum on-bank flow.

Strong tidal mixing over GB was mainly caused by shear instability of the tidal currents (i.e., shear production). The Richardson number R_i was less than 0.2 in the bottom boundary layer at the stratified site on the southern and northern flanks, and 0.1–0.2 everywhere in the vertically well-mixed crest site. A small Richardson number of less than 0.25 also was found in the upper 20 m after the maximum off-bank tidal mixing, which coincided well with timing of the relatively strong tidal mixing there.

5.2. Balance of turbulent kinetic energy

Comparison of the magnitude of terms in the turbulent kinetic energy equation revealed that the temporal variation of the turbulent kinetic energy q^2 over GB was controlled by two dominant terms: turbulent shear production (P_s) and dissipation (ε). At three selected sites on the southern, top, and northern flanks of GB, for example, P_s and ε had maximum values of about 10^{-5} W/kg at the bottom and decayed upward. P_s was balanced approximately by ε at each time step and thus on average over a tidal cycle (Fig. 17). Buoyancy production (P_b) was about one order of magnitude less than P_s, and the advection and vertical diffusion terms in the TKE equation were one or two orders of magnitude less than P_b. These relative balances were found at other sites examined over the bank. Based on these results, we conclude that tidal mixing over a 3-D GB can be generally characterized as a 1-D process with a basic local balance between shear production and dissipation.

The time variation of P_s, q^2, and P_b at these three selected sites showed that on the northern flank, the formation of the thermal depression during the offbank flow tended to create a positive P_s and a negative P_b. Since P_b was one order of magnitude smaller than P_s, remarkably strong mixing occurred during the off-bank flow due to an enhanced turbulent shear production. Near the

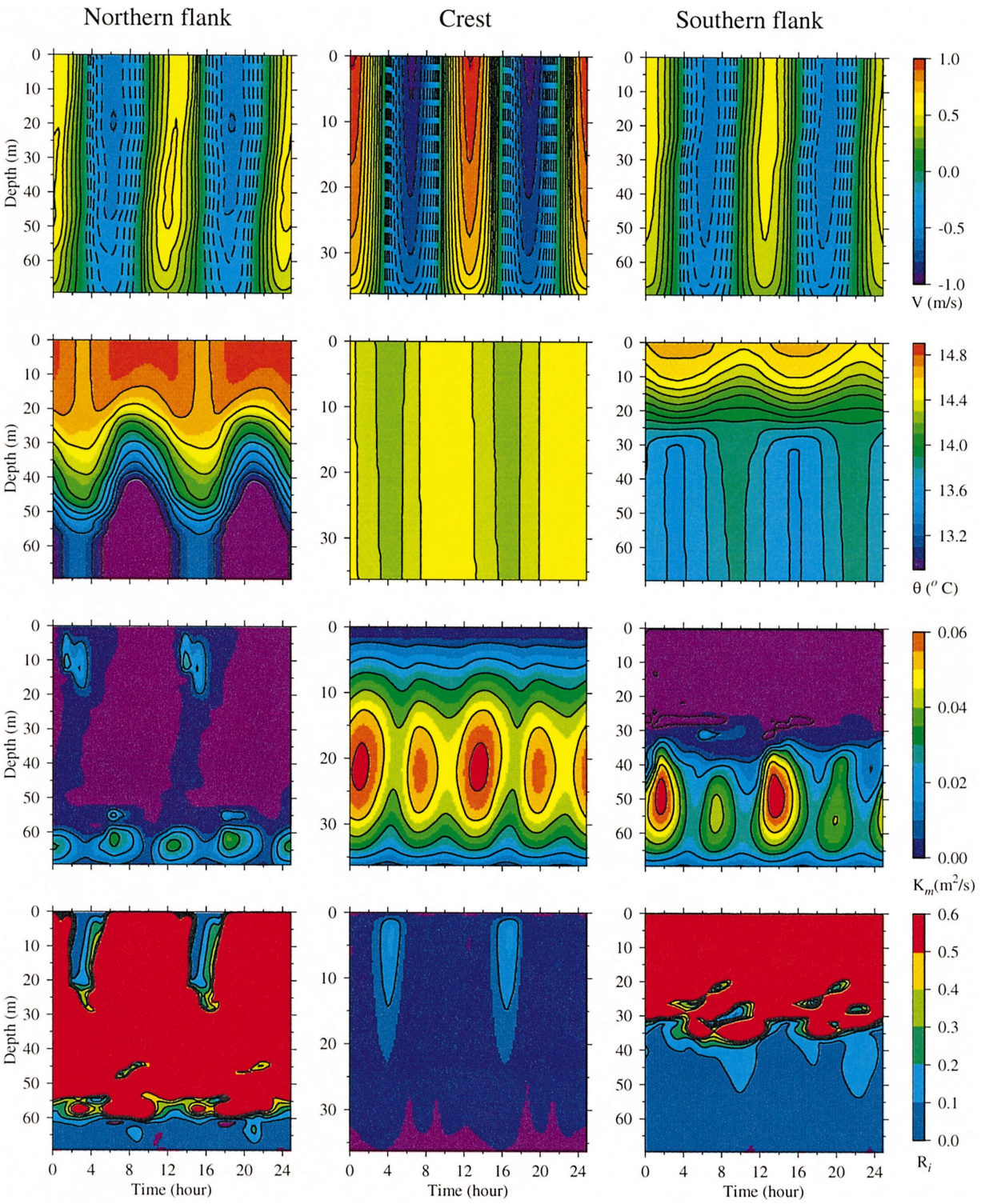
Northern flank
Crest
Southern flank
Depth (m)
Time (hour)
V (m/s)
θ (°C)
K_m(m²/s)
R_i

bottom on the southern and northern flanks, timing of stronger mixing during the on-bank flow coincided well with temporal variation of P_b. During the on-bank flow, the upslope advection of the colder water resulted in the gravitational instability and hence produced a positive P_b near the bottom. Although P_b was one order of magnitude smaller than P_s, it directly increased S_m (the stability function) and hence indirectly enhanced the vertical eddy viscosity after the maximum on-bank flow. Similar results also were evident at the crest although the water was well-mixed during most of the tidal cycle.

5.3. Comparison with observations and previous model results

The model-predicted asymmetry of tidal mixing during off- and on-bank tidal flows is evident in recent observations on the northeastern flank of GB (Yoshia and Oakey, 1996; Horne et al., 1996). This feature of tidal mixing predicted by this 3-D model was the same as that found in our 2-D experiments (C&B), and also consistent with 3-D model results presented by Naimie (1996). C&B suggested that the asymmetric tidal mixing during off- and on-bank tidal flows was caused by gravitational instability that occurred when denser (colder) water was advected upslope over lighter (warmer) water during on-bank flow. This mechanism was clearly evident in our 3-D model experiments. C&B also revealed that on the northern flank, strong vertical mixing can occur after the maximum off-bank flow as a result of a sharp thermal depression due to what appears to be like a "hydraulic jump". This feature also was found in our 3-D cases. These similarities in 2- and 3-D model results are not surprising since the dynamics of tidal mixing over the central section of GB (for these model conditions) is characterized by a local 1-D balance between turbulent shear production and dissipation.

Naimie (1996) discussed the effects of tidal time variation on tidal mixing on the northeastern flank. He proposed that relatively strong mixing could occur near the tidal transition from on-bank flow to off-bank flow (and vice versa) due to tidal straining (because the phase of tidal currents at depth leads those aloft). The vertical phase difference of tidal currents was also evident in both 2-D (C&B) and current 3-D model experiments, and supported that tidal straining also contributed to tidal mixing on Georges Bank.

Our 3-D model experiments suggest that the magnitude of ε depends sensitively on the bottom roughness z_0, with an increase in z_0 leading to an increased ε. In the case with $z_0 = 0.6$ mm everywhere and adjusted tidal amplitude on the open boundary, the model-predicted tidal-averaged ε agreed with microstructure-based estimates at two well-mixed sites on the southern (M_s) and northern (M_n) flanks (Fig. 18; see Fig. 1 for site locations). In the case with $z_0 = z_0(D)$, z_0 was equal to 10 mm at these two mixed sites. In this case, the model overestimated ε, especially at M_s (the southern flank mixed site) even though the model provided a good fit of the vertical profile of the tidal current at stations A, K, and P3.

It is not surprising that the magnitude of ε on GB is sensitive to z_0 due to the essentially 1-D nature of turbulent mixing on the bank. Increasing z_0 locally tends to enhance the vertical shear of

Fig. 16. Time series of cross-bank current (u), temperature (θ), vertical thermal diffusion coefficient (K_m), Richardson number (R_i) over two tidal cycles at the three selected sites C1 to C3 near section 1 across GB for the case with early summer stratification and tidal forcing only.

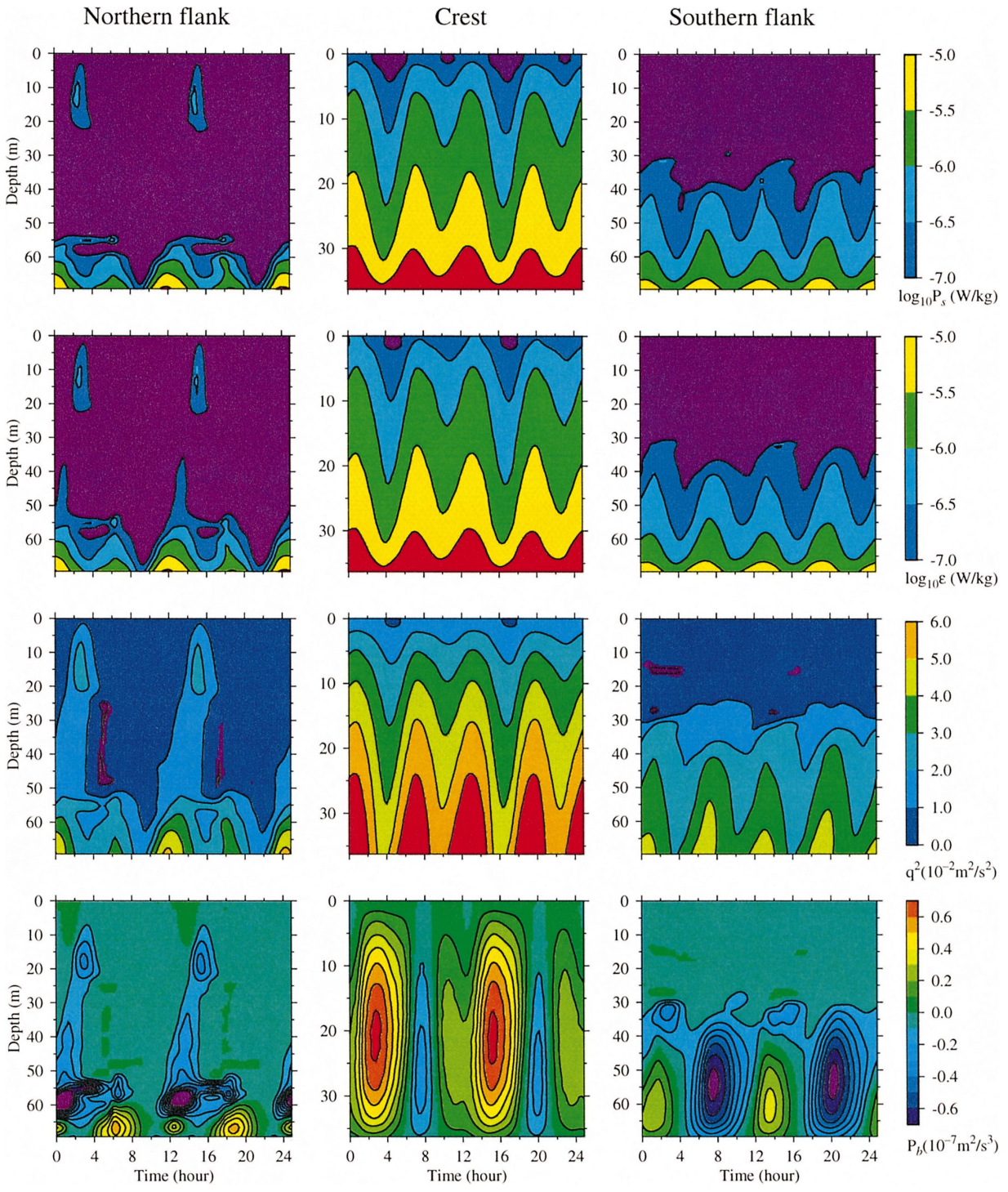

Fig. 17. Time series of turbulent shear production (P_s), dissipation (ε), kinetic energy (q^2) and buoyancy production (P_b) over two tidal cycles at the same sites C1 to C3 near section 1 for the case with early summer stratification and tidal forcing only.

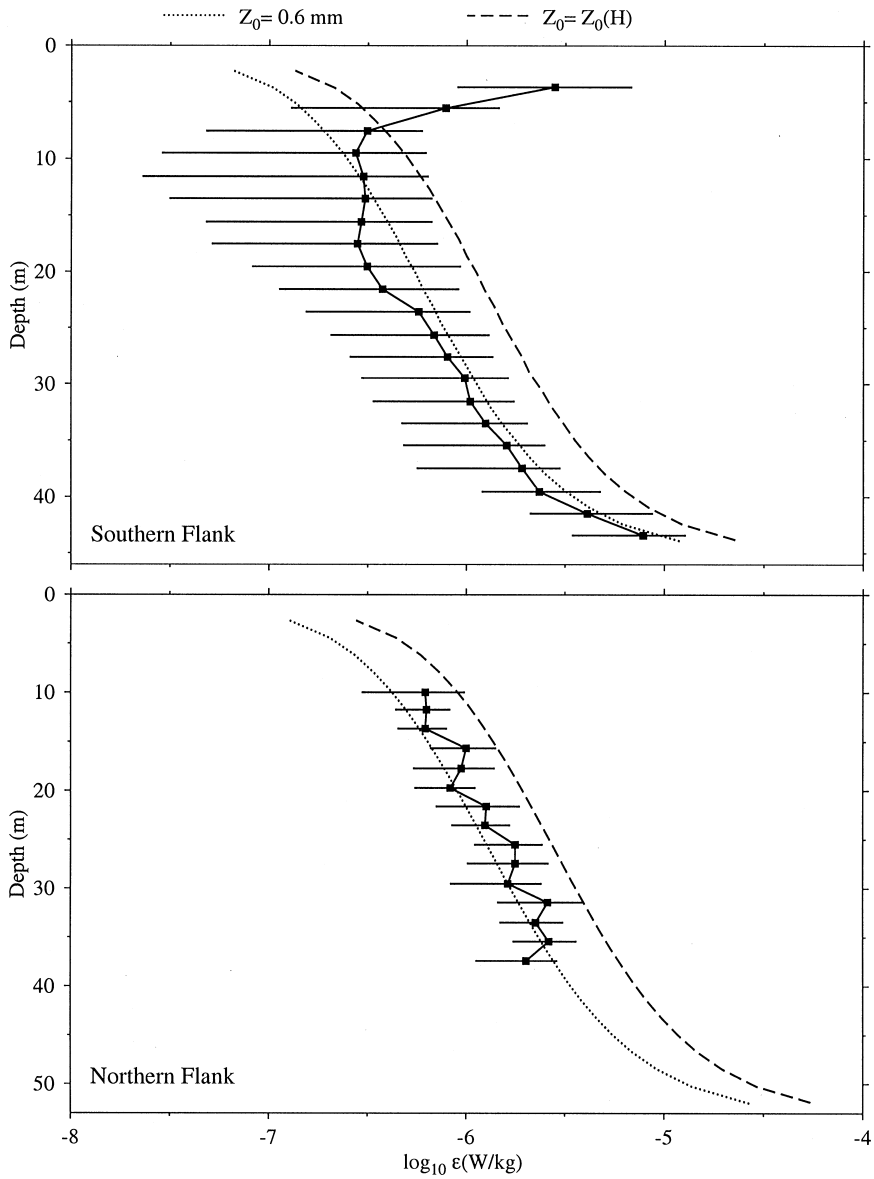

Fig. 18. Comparison between tidally averaged model (dashed lines) and turbulent dissipation rates estimated from microstructure profile measurements (solid line) at two well-mixed sites (shown as M_s and M_n in Fig. 1). The observed profiles of turbulent dissipation at the M_n and M_s with error uncertainties were digitized from Horne et al. (1996) and Burgett et al. (1996), respectively.

the tidal current, and thus result in larger P_s and ε. Since z_0 over GB is thought to vary from values like $z_0 = 0.6$ mm over the mid- and outer-shelf on the southern flank to values in excess of 10 mm over the crest of the bank, any conclusions concerning comparisons between estimated and model-predicted ε must be viewed with caution due to the significant experimental uncertainty in estimated ε and the lack of detailed knowledge of the spatial distribution of z_0.

6. Effects of high-resolution bottom topography

To examine the sensitivity of the model residual currents over GB to the spatial resolution of the bottom topography, the model runs were made using smoothed and non-smoothed bottom topographies. Smoothing was achieved using a 9-point moving average over a 3×3 array of grid points.

These two model topographies are shown in Fig. 2. For the case with early summer stratification, the model with non-smoothed bottom topography predicted many small-scale residual circulation patterns over the top of GB and at the shelf break (Fig. 19a). The water tended to flow along the small-scale local isobaths in addition to following the large-scale clockwise residual circulation around the bank. These small-scale structures were filtered out when the bottom topography was smoothed (Fig. 19b). In addition, the model revealed a relatively strong on-bank residual flow on the northwestern and northeastern flanks in the case with non-smoothed bottom topography, while the residual current mainly flowed along the bank in the case with smoothed bottom topography.

The different residual flow patterns found in these two cases suggest that over smoothing of the bottom topography may result in an unrealistic residual circulation on GB. It also may lead to an unrealistic estimation of the on-bank water transport and upwelling, particularly on the northwestern and northeastern flanks of GB. One objective of these experiments is to identify those physical processes and flow features that are robust over a range of spatial resolution in bottom topography from those which depend critically on the smallest-scale topography. We need to determine the appropriate match between grid spacing and topographic resolution for the processes being examined. The finite-element approach adopted by Lynch and co-workers provides a more flexible method to achieve this match than the simpler coordinate system that we have adopted. However, in both cases, the need to find the appropriate spatial match between grid and topographic spacing is an essential key to studying various processes.

7. The 2- and 3-D model comparison

Both the 2- and 3-D model results suggest that tidal mixing over GB is primarily driven by a local 1-D balance between turbulent shear production and dissipation. This result explains why the 2-D model was found so robust in simulating the tidal mixing front over GB (C&B, Chen et al., 1995a).

To check whether or not the 2-D model was robust to capture the basic dynamics of stratified tidal rectification on GB, we examined the momentum balance along the cross-bank section 1 (shown in Fig. 1) for the 3-D case with smoothed bottom topography. In the case with early summertime stratification, the model-predicted 3-D stratified residual circulation over GB exhibited an equilibrium momentum balance between (1) cross-bank and vertical advection, (2) Coriolis acceleration, and (3) vertical diffusion in the along-bank (x) direction, and between (1) cross-bank and vertical advection, (2) Coriolis acceleration, (3) vertical diffusion, and (4) cross-bank gradients of the surface elevation in the cross-bank (y) direction (Fig. 20). The along-bank gradient of baroclinic pressure was too weak to be dynamically important. The along-bank gradient of the surface elevation was one order of magnitude smaller than the cross-bank momentum advective

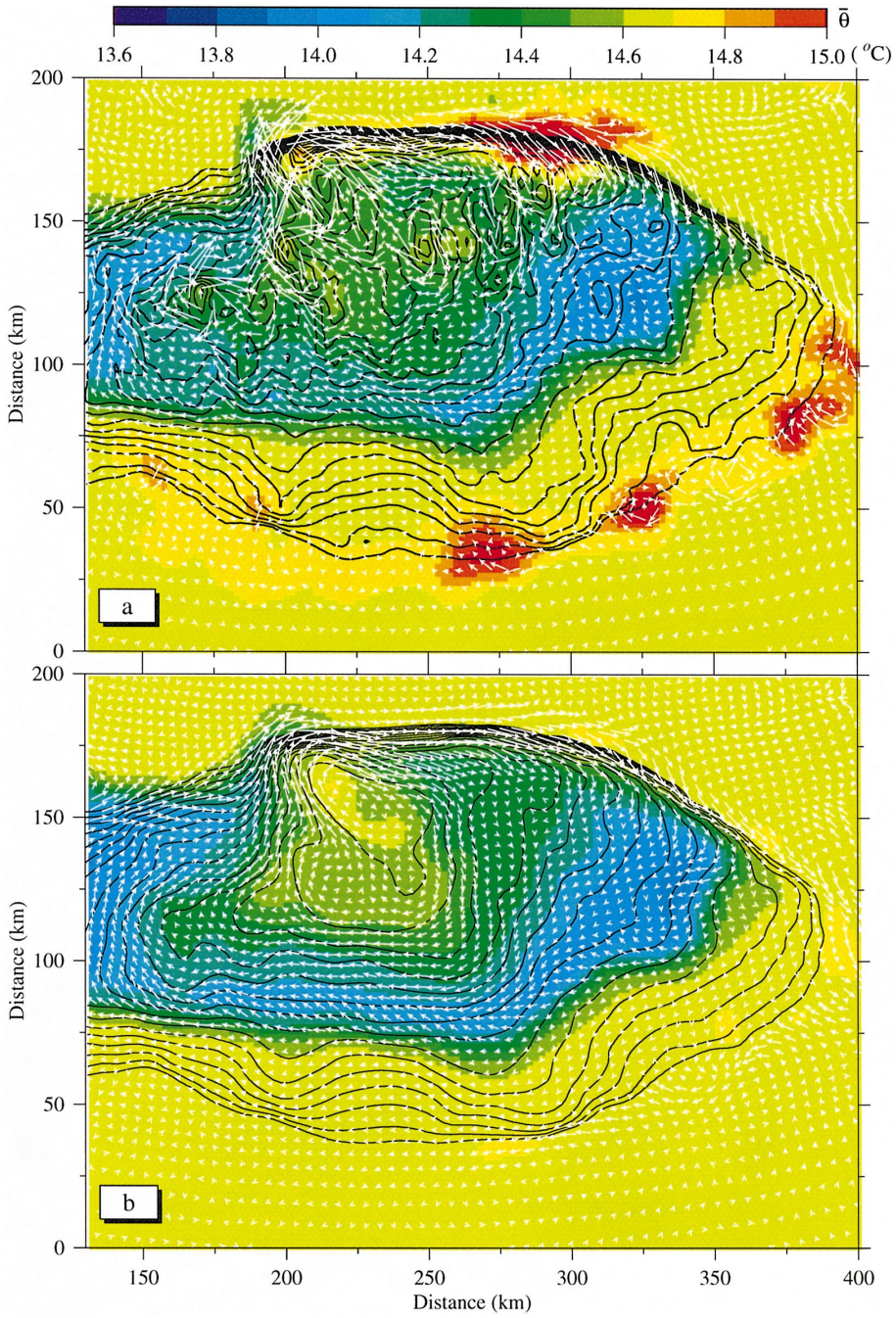

Fig. 19. The surface distributions of temperature and residual current vectors over Georges Bank for the cases with non-smoothed (a) and smoothed (b) bottom topographies.

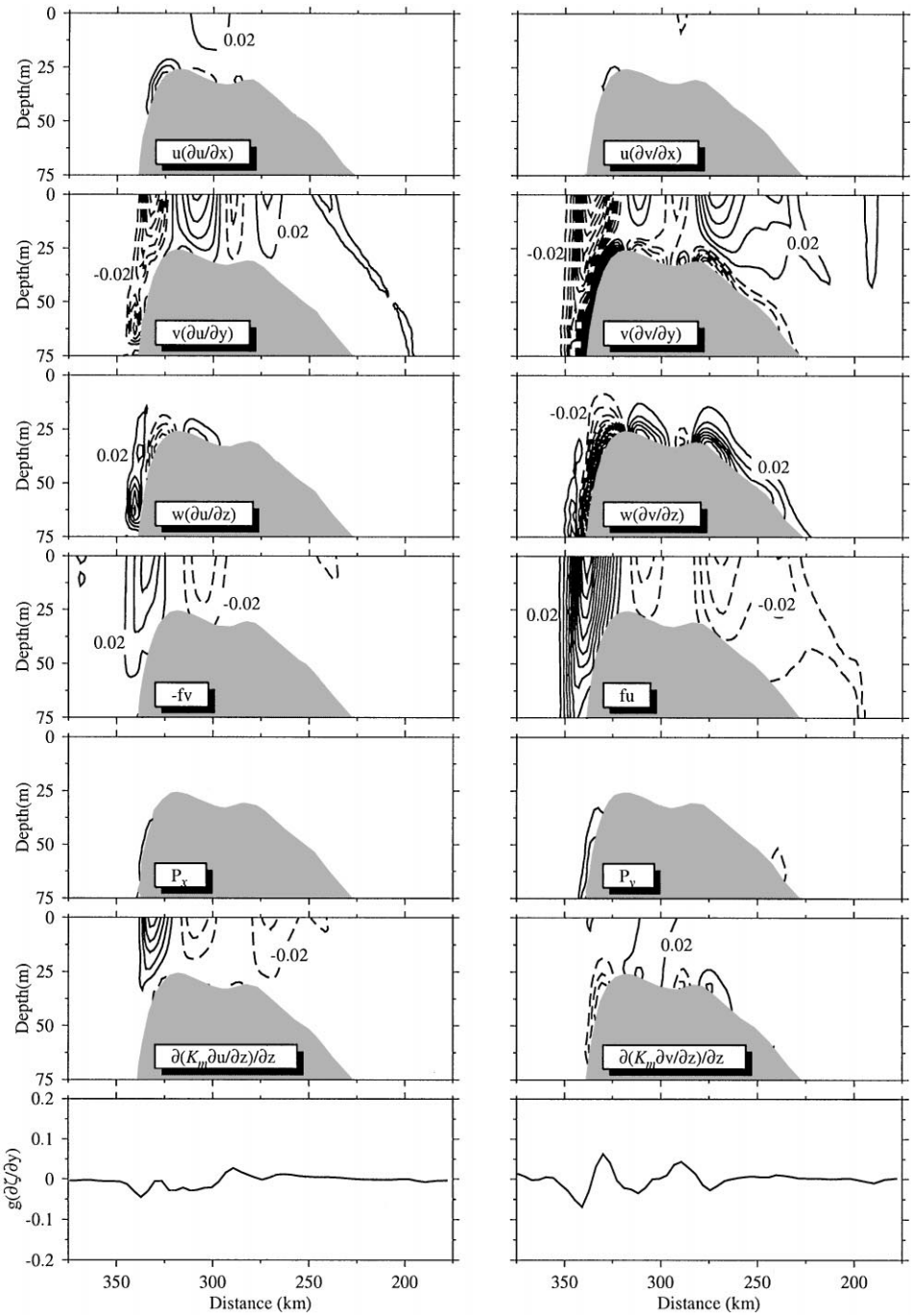

Fig. 20. Cross-bank distributions of terms in the mean momentum equations for the case with early summer stratification and only tidal forcing. The contour interval is $0.01 \times 10^{-4}\,\mathrm{m/s^2}$.

term $v\partial u/\partial y$. Also, the along-bank advective terms $u\partial u/\partial x$ and $u\partial v/\partial x$ were smaller except near the bottom of the steep northern slope where they were noticeable. To first order, the terms $\partial P/\partial x$, $g\partial\zeta/\partial x$, $u\partial u/\partial x$, and $u\partial v/\partial x$ can be ignored if the study was only focused on the frontal circulation around the bank. This suggests that a 2-D model without the inclusion of along-bank variation should be sufficiently robust to capture the basic process of stratified tidal rectification across GB (Chen et al., 1995a).

8. Discussion

Our 3-D model experiments have revealed that tidal simulation and tidal mixing depend sensitively on the bottom roughness parameter z_0. This implies that a successful model for GB should be capable of simulating not only tidal elevation and currents but also turbulent properties. One of the goals of the US GLOBEC/Georges Bank Program is to study the cross-frontal water transport over GB. To achieve this goal, one needs to know quantitatively the cross-frontal Lagrangian circulation. Accurate estimation of the cross-frontal Lagrangian trajectories can only be made when we can accurately predict the cross-bank tidal current and secondary residual circulation. Previous studies have suggested that the pattern of cross-frontal secondary circulation over GB depended critically on the turbulence parameterization (Wright and Loder, 1985). Our model experiments with the MY2.5 turbulent closure scheme show that the simulation of turbulent properties over GB is quite sensitive to the choice of z_0. It may be a bit premature to make any positive or negative conclusions about the capability of MY2.5 to simulate complex flows in coastal regions where z_0 can be quite variable.

On the other hand, our 3-D model has shown a reasonable simulation of tidal currents over GB and turbulent properties in the mixed region of GB. Results from the 3-D model suggest that the patterns of secondary cross-bank circulation vary significantly with different bottom topographic slope, tidal mixing, and advection. A schematic of cross-bank secondary residual circulation is shown in Fig. 21 with an understanding that these patterns may be only qualitatively meaningful.

On the southern flank, the model predicted upwelling almost throughout the water column from the bottom at the tidal mixing front and from the deeper region along isopycnals at the top of the bottom boundary layer (Figs. 21a, 12 and 13). This upwelled water diverged into both the well-mixed and stratified sides of the front near the surface. A near-surface convergence region existed on the stratified side and at the lower part of the saddle zone at the top of the bottom boundary layer near the front. In the stratified region where the water depth was deeper than 75 m, the cross-bank current was characterized by multiple closed-circulation cells. The model also suggested a cross-frontal on-bank current near the bottom.

On the northern flank, the model predicted closed secondary circulation cells with a divergence near the bottom on the slope and a convergence toward the front near the surface (Figs. 21b, 12 and 13). A center of the convergence area was located at the axis of the maximum along-bank residual current. A cross-frontal on-bank residual flow was found near the bottom on the northern edge of the bank.

On the northeastern flank (along section 2 shown in Fig. 1), the pattern of the secondary residual circulation was similar to that on the northern flank but with an opposite current direction. The current diverged on both sides of the axis of the maximum along-bank flow at the front near the

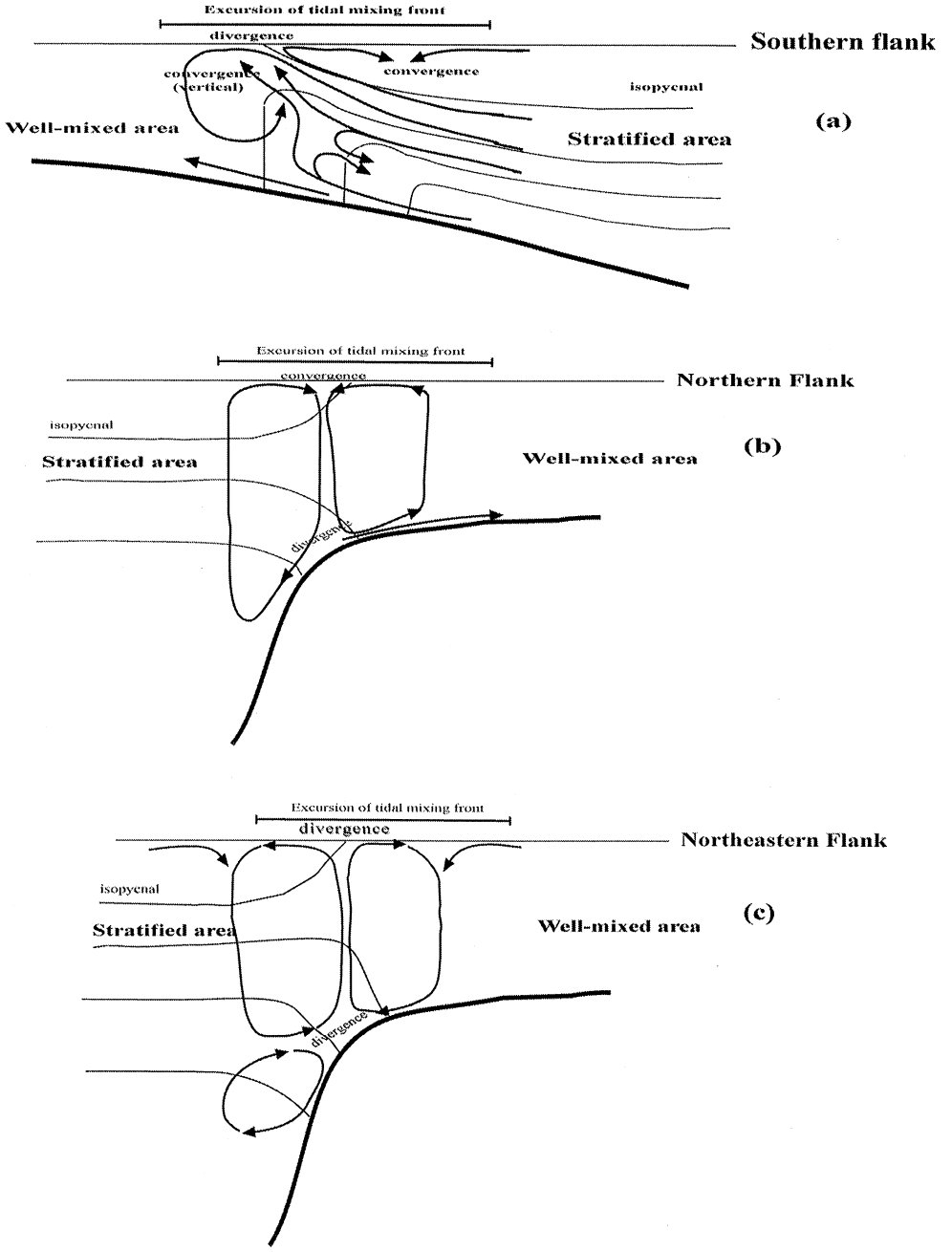

Fig. 21. Schematic of model-predicted, cross-frontal secondary residual circulation on the southern (a), northern (b) and northeastern (c) flanks of Georges Bank based on runs with non-smoothed topography, early summer stratification, and tidal forcing only.

surface and converged at a depth of 75 m at the edge of the bank (Figs. 21c and 14). The surface convergence zone was located in both stratified and mixed regions. A saddle point may exist near the bottom of the slope between 75 and 90 m, which can lead to a chaotic cross-frontal water exchange near the bottom (Chen, 2000).

It should be pointed out here that the patterns of cross-frontal secondary residual circulation summarized here are based on the distributions of the Eulerian residual current on sections 1 and 2 (Fig. 1). The Lagrangian residual circulation pattern on GB might differ significantly from the Eulerian residual circulation, especially on the northern and northeastern flanks (C&B). The reality of these circulation patterns needs to be verified directly from current measurements. Also, the along-bank residual current, in general, is one order of magnitude larger than the cross-bank residual current. The 3-D nature of the residual circulation needs to be considered when cross-frontal water exchange is estimated

9. Summary

The influence of tidal and wind mixing on circulation and stratification over Georges Bank (GB) and adjacent coastal regions of the Gulf of Maine (GOM) has been examined using a 3-D semi-implicit version of the Blumberg and Mellor (1987) primitive equation ocean circulation model with MY2.5 turbulent closure. The numerical domain covered the GOM/GB region with an open boundary starting at the New Jersey coast and ending at the Nova Scotia coast. The model provided a reasonable simulation of the M_2 tidal elevation and phase. The model run as an initial value problem with early summer stratification exhibited tidal mixing fronts around the 40–60 m isobaths over GB and Nantucket Shoals (NS), and 100-m isobath on Browns Bank (BB).

The formation of tidal mixing fronts significantly enhanced the along-bank tidal rectified current over GB and adjacent coastal regions. Over GB, the along-bank current increased to 30 cm/s on the northwest flank, 20–25 cm/s on the northern flank, and 5–8 cm/s on the southern flank. The model predicted three main re-circulation paths of the stratified residual flow on the northeastern flank of GB: (1) along the 40-m isobath; (2) between the 40–60 m isobaths; and (3) along the 100-m isobath. The model-predicted pattern of residual circulation over GB was qualitatively (and to a certain extent quantitatively) in good agreement with previous moored current meter and drifter measurements.

The model predicted cooler water temperatures within the tidal mixing front near the 60-m isobath along the eastern and southern flank of GB and in the shallow region of less than 60 m over NS. These cold water zones tended to become cooler due to summer mean wind-induced mixing and upwelling. The model-predicted location of the tidal mixing front and spatial distribution of stratification were in good agreement with satellite sea-surface temperature (SST) images for GB and were consistent with predictions made using the Simpson and Hunter (1974) energy argument.

The 3-D model simulations showed that tidal mixing and turbulent dissipation exhibit temporal and spatial asymmetries over GB. For the simple initial conditions used in our experiments, tidal mixing over GB can be characterized to lowest order by a 1-D local balance between turbulent-shear production and dissipation. The magnitudes of turbulent-shear production and dissipation clearly depend critically on the bottom roughness.

The analysis of the momentum balance across the center section of GB in the 3-D model case suggests that as a first-order approximation, the 2-D model captures the basic dynamics of the tidal mixing front over GB. The numerical experiments with non-smoothed and smoothed bottom topography indicate that over-smoothing of the bottom topography leads to a smoothed residual circulation over GB, which may miss important smaller-scale circulation and mixing features. For example, the qualitative nature of the on-bank water transport and upwelling, particularly on the northwestern and northeastern flanks of GB, differed significantly between the smoothed and non-smoothed cases. Additional research, including field measurements, is needed to determine which flow pattern is more realistic, although we suggest the non-smoothed results are probably closer to nature.

The model results suggest that the pattern of the cross-bank secondary residual circulation varies significantly with different bottom topographic slope, tidal mixing, and advection. On the southern flank, the cross-frontal secondary circulation was characterized by multiple circulation cells, with a divergence at the edge of the front near the surface. On the northern flank, the model predicted closed secondary circulation cells, with a convergence toward the front near the surface and a divergence near the bottom on the slope. On the northeastern flank, the current tended to diverge toward both sides of the maximum along-bank current jet near the surface and converge at a depth of 75 m near the bottom of the slope.

We have attempted in the past to use a 2-D primitive equation ocean circulation model to study several basic processes occurring on GB associated with tidal forcing and stratification. In particular, these processes include the formation of tidal mixing fronts, stratified tidal rectification, and secondary circulation. This paper introduces a 3-D model with identical physics and more realistic GB topography, in order to allow us to continue process-oriented modeling with processes which inherently result in 3-D flows (e.g., surface heating and cooling, wind forcing, and upstream forcing on the Scotian Shelf). While serious concerns have been raised by Stacey et al. (2000) about the ability of the MY2.5 turbulence closure scheme to deal with internal mixing and the vertical transport of turbulent kinetic energy away from the bottom boundary, we have and will continue to use the MY2.5 scheme as the best of the presently available models for turbulent processes for these kind of idealized process-oriented numerical studies. Our next study will focus on the effects of the diurnal summer heat flux and mean summer winds on the tidal residual circulation over GB presented here.

Acknowledgements

This research was supported by the US GLOBEC Northwest Atlantic/Georges Bank program through NOAA grants NA56RG0487, NA960P003, and NA960P005 to Changsheng Chen, NSF grants OCE96-32357 and OCE98-06379 to Robert Beardsley, and NOAA grant NA76GP0176 to Peter Franks. We want to thank Hui Tian for his assistance in grid generation, digitizing the amplitudes and phases of the tidal elevation used on the open boundary, and obtaining the turbulent dissipation data used for the model-data comparison. Two anonymous reviewers provided many critical comments and constructive suggestions, which helped to improve and clarify the final manuscript. The US GLOBEC contribution number is 147.

References

Bigelow, H.B., 1927. Physical oceanography of the Gulf of Maine. US Fisheries Bulletin 40, 511–1027.
Blumberg, A.F., 1994. A primer for ECON-si. Technical Report, HydroQual, Inc., Mahwah, NJ, 66pp.
Blumberg, A.F., Mellor, G.L., 1987. A description of a three-dimensional coastal ocean circulation model. Three Dimensional Coastal Models, Coastal and Estuarine Sciences, 5, N. Heaps (ed.), American Geophysical Union 1–16.
Brown, W.S., 1984. A comparison of Georges Bank, Gulf of Maine and New England Shelf tidal dynamics. Journal of Physical Oceanography 14, 145–167.
Burgett, R., 1997. The structure of tidal mixing on the southern flank of Georges Bank. M.S. Thesis, University of Rhode Island, 142pp.
Burgett, R., Hebert, D., Oakey, N., 1996. U.S. GLOBEC Georges Bank microstructure data. University of Rhode Island GSO Technical Report No. 96-6, 414pp.
Butman, B., Beardsley, R.C., Magnell, B., Frye, D., Vermersch, J.A., Schlitz, R., Limeburner, R., Wright, W.R., Noble, M.A., 1982. Recent observations of the mean circulation on Georges Bank. Journal of Physical Oceanography 12, 569–591.
Butman, B., Fry, V., 1990. Atlas of tidal elevation and moored current observations in Massachusetts and Cape Cod Bays, 1970–1989. Open File Report, US Geological Survey, Branch of Atlantic Marine Geology, Woods Hole, MA 02543, 69pp.
Casulli, V., 1990. Semi-implicit finite-difference methods for the two-dimensional shallow water equations. Journal of Computational Physics 86, 56–74.
Chen, C., 2000. Possible chaotic transport across coastal fronts. Unpublished manuscript.
Chen, C., Beardsley, R.C., 1995. A numerical study of stratified tidal rectification over finite-amplitude banks. Part I: symmetric bank. Journal of Physical Oceanography 25 (9), 2090–2110.
Chen, C., Beardsley, R.C., 1998. Tidal mixing over a finite amplitude asymmetric bank: a model study with application to Georges Bank. Journal of Marine Research 56, 1163–1201.
Chen, C., Beardsley, R.C., Limeburner, R., 1995a. A numerical study of stratified tidal rectification over finite-amplitude banks. Part II: Georges Bank. Journal of Physical Oceanography 25 (9), 2111–2128.
Chen, C., Beardsley, R.C., Limeburner, R., 1995b. Variability of currents in late spring in the northern Great South Channel. Continental Shelf Research 15, 451–473.
Chen, C., Beardsley, R.C., Limeburner, R., 1995c. Variability of water properties in late spring in the northern Great South Channel. Continental Shelf Research 15, 415–431.
Chen, C., Beardsley, R.C., Franks P.J., 2000. Influences of heat flux on the 3-D circulation and stratification over Georges Bank. Journal of Geophysical Research, submitted.
Churchill, J.H., Manning, J.P., 1997. Horizontal convergence and dispersion over the southern flank of Georges Bank. ICES 1997 Annual Science Conference (85th Statutory Meeting), Baltimore, Maryland, USA, 25–30 September, 1997.
Egbert, G.D., Bennett, A.F., Foreman, M.G.G., 1994. TOPEX/POSEIDON tides estimated using a global inverse model. Journal Geophysical Research 99, 24821–24852.
Franks, P.S.J., Chen, C., 1996. Plankton production in tidal fronts: a model of Georges Bank in summer. Journal of Marine Research 54, 631–651.
Franks, P.S.J., Chen, C., 2001. A 3-D prognostic numerical model study of the Georges Bank ecosystem. Part II: biological–physical model. Deep-Sea Research II 48, 457–482.
Galperin, B., Kantha, L.H., Hassid, S., Rosati, A., 1988. A quasi-equilibrium turbulent energy model for geophysical flows. Journal of Atmospheric Sciences 45, 55–62.
Greenberg, D.A., 1983. Modeling the mean barotropic circulation in the Bay of Fundy and Gulf of Maine. Journal of Physical Oceanography 13, 886–904.
Haney, R.L., 1991. On the pressure gradient force over steep topography in sigma-coordinate ocean model. J. Phys. Oceanogr. 21, 610–619.
Horne, E.P.W., Loder, J.W., Naimie, C.E., Oakey, N.S., 1996. Turbulence dissipation rates and nitrate supply in the upper water column on Georges Bank. Deep-Sea Research 43, 1683–1712.
Large, W.S., Pond, S., 1981. Open ocean momentum flux measurements in moderate to strong winds. Journal of Physical Oceanography 11, 324–406.

Limeburner, R., Beardsley, R.C., 1996. Near-surface recirculation over Georges Bank. Deep-Sea Research 43 (7–8), 1547–1574.

Loder, J.W., 1980. Topographic rectification of tidal current on the sides of Georges Bank. Journal of Physical Oceanography 10, 1399–1416.

Loder, J.W., Greenberg, D.A., 1986. Predicted positions of tidal fronts in the Gulf of Maine region. Continental Shelf Research 6, 397–414.

Loder, J.W., Wright, D.G., 1985. Tidal rectification and front circulation on the sides of Georges Bank. Journal of Marine Research 43, 581–604.

Lynch, D.R., Naimie, C.E., 1993. The M_2 tide and its residual on the outer bank of the Gulf of Maine. Journal of Physical Oceanography 23, 2222–2253.

Mellor, G.L., Yamada, T., 1974. A hierarchy of turbulence closure models for planetary boundary layers. Journal of Atmospheric Sciences 33, 1791–1896.

Mellor, G.L., Yamada, T., 1982. Development of a turbulence closure model for geophysical fluid problem. Review of Geophysical and Space Physics 20, 851–875.

Moody, J.A., Butman, B., Beardsley, R.C., Brown, W.S., Daifuku, P., Irish, J.D., Mayer, D.A., Mofjelf, H.O., Petrie, B., Ramp, S., Smith, P., Wright, W.R., 1984. Atlas of tidal elevation and current observations on the northeast American continental shelf and slope. US Geological Survey Bulletin 1611, 122pp.

Naimie, C.E., 1996. Georges Bank residual circulation during weak and strong stratification periods: prognostic numerical model results. Journal of Geophysical Research 101 (C3), 6469–6486.

Naimie, C.E., Loder, J.W., Lynch, D.R., 1994. Seasonal variation of the three-dimensional residual circulation on Georges Bank. Journal of Geophysical Research 99 (C8), 15967–15989.

Roworth, E., Signell, R., 1998. Construction of digital bathymetry for the Gulf of Maine. (See http:/orale.er.usgs.gov/GoMaine/bathy/index.htm).

Simpson, J.H., Hunter, J.R., 1974. Fronts in the Irish Sea. Nature 250, 404–406.

Stacey, M.T., Monismith, S.G., Burau, J.R., 2000. Measurements of Reynolds stress profiles in unstratified tidal flow. Journal of Geophysical Research, submitted for publication.

Werner, S., Beardsley, R.C., 2000. The vertical structure of the tidal boundary layer on the southern flank of Georges Bank during near-homogenous winter conditions. Journal of Geophysical Research, submitted for publication.

Yoshia, J., Oakey, N.S., 1996. Characterization of vertical mixing at a tidal-front on Georges Bank. Deep-Sea Research 43, 1713–1744.